

1 **Export fluxes in a naturally iron-fertilized area of the Southern**
2 **Ocean, ~~the Kerguelen Plateau~~: importance of diatom spores and**
3 **faecal pellet for export ~~and ecological vectors of carbon and~~**
4 **~~biogenic silica to depth~~ (part 2).**

5 M. Rembauville^{1,2}, S. Blain^{1,2}, L. Armand³, B. Quéguiner⁴ and I. Salter^{1,2,5}

6 ¹ Sorbonne Universités, UPMC Univ Paris 06, UMR 7621, LOMIC, Observatoire Océanologique, Banyuls-sur-
7 Mer, France.

8
9 ² CNRS, UMR 7621, LOMIC, Observatoire Océanologique, Banyuls-sur-Mer, France.

10
11 ³ Department of Biological Sciences and Climate Futures, Macquarie University, New South Wales, Australia

12

13 ⁴ Aix-Marseille Université, Université de Toulon, CNRS/INSU, IRD, MOI, UM 110, Marseille, France.

14

15 ⁵ Alfred-Wegener-Institute for Polar and Marine research, Bremerhaven, Germany.

16

17 Correspondance to : M. Rembauville (rembauville@obs-banyuls.fr).

18

19

20 **Abstract**

21 ~~The chemical (particulate organic carbon and nitrogen, biogenic silica) and biological~~

22 ~~(diatoms and faecal pellets)~~ The biological composition of the material exported to a moored

23 sediment trap located under the winter mixed layer of the naturally-fertilized Kerguelen

24 Plateau in the Southern Ocean was studied over an annual cycle. Despite iron availability in

25 spring, the annual particulate organic carbon (POC) export (98.2 mmol m⁻²) at 289 m was low

26 but annual biogenic silica export was significant (114 mmol m⁻²). This feature was related to

27 the abundance of empty diatom ~~frustules cells~~ and the ratio of full:empty cells exerted a first

28 order control in BSi:POC export stoichiometry of ~~the~~ biological pump. *Chaetoceros*

29 *Hyalochaete* spp. and *Thalassiosira antarctica* resting spores were responsible for more than

30 60 % of the annual POC flux that occurred during two very short export events of <14 days in

31 spring-summer. (~~≤14 days in spring-summer~~) representing the majority of captured export.
32 **Relatively** low diatom fluxes were observed over the remainder of the year. Faecal pellet
33 contribution to annual carbon flux was low (34 %) and reached ~~it's~~ **its** seasonal maximum in
34 autumn and winter (> 80 %). The seasonal progression of faecal pellet types revealed a clear
35 transition from small spherical shapes (small copepods) in spring, larger cylindrical and
36 ellipsoid shapes in summer (euphausiids and large copepods) and finally large tabular shapes
37 (salps) in autumn and winter. We propose ~~that~~ in this High Biomass, Low Export (HBLE)
38 environment **that** small, highly silicified, fast-sinking resting spores are able to bypass the
39 **high intense** grazing pressure and efficient carbon transfer to higher trophic levels that are
40 responsible for the low fluxes observed the during the remainder of the year. **More generally**
41 ~~Our~~ study also provides a statistical framework linking the ecological succession of diatom
42 and zooplankton communities to the seasonality of carbon and silicon export within an iron-
43 fertilized bloom region in the Southern Ocean.

44

45 **1 Introduction**

46 The Southern Ocean is the place of exposure of old upwelled waters to the atmosphere and
47 the formation of ~~medal~~ **mode** waters, thereby ventilating an important part of the global
48 Ocean and playing a central role in distributing heat, carbon and nutrients in the global Ocean
49 (Sarmiento et al., 2004; Takahashi et al., 2012; Sallée et al., 2012). Silicon trapping occurs in
50 the Southern Ocean because silicon is stripped out of the euphotic zone more efficiently than
51 phosphorous and nitrogen (Holzer et al., 2014). It is generally acknowledged that regional
52 variations in plankton community structure are responsible for variations in nutrient
53 stoichiometry in the Southern Ocean (Jin et al., 2006; Weber and Deutsch, 2010) and that the
54 biological pump is a central process regulating this stoichiometry (Ragueneau et al., 2006;
55 Salter et al., 2012; Primeau et al., 2013). These characteristics emphasize the importance of
56 biological processes in the Southern Ocean waters for the availability of silicic acid and
57 nitrate (Sarmiento et al., 2004; Dutkiewicz et al., 2005) as well as phosphate (Primeau et al.,
58 2013) at lower latitudes, thereby regulating part of the productivity of the global Ocean. It has
59 been proposed that change in the uptake ratio of silicate and nitrate by Southern Ocean
60 phytoplankton in response to increased iron availability during the Last Glacial Maximum
61 could have played a substantial role in varying atmospheric CO₂ (Brzezinski et al., 2002;
62 Matsumoto et al., 2002).

63 Primary production in the Southern Ocean is regulated by macro- and micronutrients
64 availability (Martin et al., 1990; Moore et al., 2001; Nelson et al., 2001; Moore et al., 2013)
65 and light-mixing regime (Venables and Moore, 2010; Blain et al., 2013). The complex
66 interaction of these factors introduces strong spatial heterogeneity in the distribution of
67 primary producer biomass (Arrigo et al., 1998; Thomalla et al., 2011). In particular, High
68 Nutrient, Low Chlorophyll (HNLC) areas in the open ocean contrast strongly with highly
69 productive, naturally fertilized, blooms located downstream of island systems such as the

70 Kerguelen Plateau (Blain et al., 2001, 2007), Crozet Islands (Pollard et al., 2002) and South
71 Georgia (Park et al., 2010; Tarling et al., 2012). The diatom-dominated phytoplankton blooms
72 characteristic of these island systems are the product of multiple environmental conditions
73 favorable for their rapid growth (Quéguiner, 2013), which appear to promote POC export
74 from the mixed layer (Nelson et al., 1995; Buesseler, 1998). However the ecological traits of
75 certain species can impact the BSi:POC export stoichiometry (Crawford, 1995; Salter et al.,
76 2012), and may therefore control the biogeochemical function of a particular region of the
77 Southern Ocean (Smetacek et al., 2004; Assmy et al., 2013)

78 Among the numerous ecological characteristics of plankton communities, algal
79 aggregation (Jackson et al., 2005; Burd and Jackson, 2009), mesozooplankton faecal pellets
80 (Lampitt et al., 1990; Wilson et al., 2008, 2013), vertical migrations of zooplankton and
81 mesopelagic fish (Jackson and Burd, 2001; Steinberg et al., 2002; Davison et al., 2013),
82 radiolarian faecal pellets (Lampitt et al., 2009), and diatom resting spore formation, (Salter et
83 al., 2012; Rynearson et al., 2013) have all been highlighted as efficient vectors of carbon
84 export out of the surface mixed layer. The challenge in describing the principal ecological
85 processes regulating POC export fluxes is the requirement to have direct access to sinking
86 particles. Many of the processes described occur in the upper layers of the ocean, where
87 circulation can strongly influence the reliability of sediment trap collections (Baker et al.,
88 1988; Buesseler et al., 2007). Short term deployments of free drifting sediment traps can be an
89 efficient solution to minimize the hydrodynamic bias (Buesseler et al., 2000; Lampitt et al.,
90 2008) but spatial and temporal decoupling of production and export needs to be considered
91 (Salter et al., 2007; Rynearson et al., 2013). In regions characterized by relatively weak
92 circulation, moored sediment trap observations in areas of naturally fertilized production can
93 track temporal succession of exported material from long-term (several month) blooms
94 (Westberry et al., 2013). Such an approach can partially resolve how ecological processes in

95 plankton communities regulate POC and biomineral export out of the mixed layer (Salter et
96 al., 2012; Salter et al., 2014), although selective processes during export may modify original
97 surface features

98 The central Kerguelen Plateau is a good environment to study the ecological vectors of
99 export with sediment traps due to the naturally fertilized recurrent bloom (Blain et al., 2007)
100 and shallow bathymetry that breaks the strong Antarctic Circumpolar Current flow (Park et
101 al., 2008, 2014). As reported in the companion paper (Rembauville et al., 2014), annual POC
102 export measured by the sediment trap deployment at 289 m beneath the southeastern iron-
103 fertilized Kerguelen bloom is $98 \pm 4 \text{ mmol m}^{-2} \text{ y}^{-1}$. This downward flux of carbon may account
104 for as little as $\sim 1.5 \%$ of seasonal net community carbon production ($6.6 \pm 2.2 \text{ mol m}^{-2}$,
105 Jouandet et al., 2008) and $< 2 \%$ of seasonally integrated POC export estimated at 200 m from
106 a dissolved inorganic carbon budget (5.1 molC m^{-2} ; Blain et al., 2007). ~~A comparison of POC~~
107 ~~fluxes over short term intervals (<1 month) from a wide variety of approaches revealed~~
108 ~~similar reductions in POC flux between 200 m and 300 m during spring and summer~~
109 ~~(Rembauville et al., 2014). Such a rapid attenuation of flux appears to be inconsistent with~~
110 ~~microbial remineralization of settling particles (Rembauville et al., 2014). Although~~
111 ~~hydrodynamical and biological biases related to the shallow moored sediment trap~~
112 ~~deployment may partly explain the low POC fluxes we report, independent measurements of~~
113 ~~low POC fluxes (>300 m) at the same station (Ebersbach and Trull, 2008; Jouandet et al.,~~
114 ~~2014) are consistent with the hypothesis of an intense flux attenuation below the winter mixed~~
115 ~~layer. Previously, we have suggested the role of higher trophic levels (mesozooplankton and~~
116 ~~mesopelagic fish) feeding at the base of the mixed layer as an explanation for the low POC~~
117 ~~fluxes we observed. The intense microbial heterotrophic activity (Obernosterer et al., 2008;~~
118 ~~Christaki et al., 2014) and zooplankton grazing (Carlotti et al., 2008, 2015) in the mixed layer,~~
119 ~~together with the strong flux attenuation at depth lead to a~~ These observations suggest a ‘High

120 Biomass, Low Export' (HBLE, Lam and Bishop, 2007) ~~status environment~~ characterizing the
121 productive Kerguelen Plateau. ~~HBLE~~ status appears to be a common feature of other
122 productive sites of the Southern Ocean (Lam and Bishop, 2007; Ebersbach et al., 2011; Lam
123 et al., 2011; Maiti et al., 2013; ~~Cavan et al., 2015~~). Describing the temporal succession of
124 POC and BSi flux vectors from the Kerguelen Plateau is of interest to increase our
125 understanding of the ecological processes characterizing HBLE environments. ~~In particular,~~
126 ~~phytoplankton community composition and faecal pellet fluxes may be a significant~~
127 ~~component of particles exported from the Kerguelen Plateau.~~

128 ~~Numerous Several~~ studies have described diatom fluxes from sediment trap records in
129 the Southern Ocean (Leventer and Dunbar, 1987; Fischer et al., 1988; Abelmann and
130 Gersonde, 1991; Leventer, 1991; Gersonde and Zielinski, 2000; Fischer et al., 2002; Pilskaln
131 et al., 2004; Ichinomiya et al., 2008; Salter et al., 2012). Highest diatom fluxes recorded by
132 sediment traps ($> 10^9$ ~~cells valves~~ $m^{-2} d^{-1}$) ~~are were~~ observed in the Seasonal Ice Zone (SIZ)
133 near Prydz Bay and Adélie Land and ~~are were~~ dominated by *Fragilariopsis kerguelensis* and
134 ~~smaller Fragilariopsis species such as Fragilariopsis curta and Fragilariopsis cylindrus~~
135 (Suzuki et al., 2001; Pilskaln et al., 2004). These high fluxes occurred in ~~spring summer~~ and
136 ~~are were~~ associated with the melting of sea ice. Changes in light availability and melt water
137 input appear to establish favorable conditions for the production and export of phytoplankton
138 cells (Romero and Armand, 2010). In the Permanently Open Ocean Zone (POOZ), ~~highest~~
139 diatom fluxes ~~recorded are were~~ two orders of magnitude lower $\sim 10^7$ ~~cell valves~~ $m^{-2} d^{-1}$
140 (Abelmann and Gersonde, 1991; Salter et al., 2012; Grigorov et al., 2014) and typically
141 represented by *F. kerguelensis* and *Thalassionema nitzschioides*. ~~One notable exception is~~
142 ~~except in~~ the naturally ~~iron~~ fertilized waters downstream of the Crozet Plateau where resting
143 spores of *Eucampia antarctica* var. *antarctica* dominated the diatom export assemblage
144 (Salter et al., 2012)

145 Other studies have reported ~~the~~ faecal pellet contribution to POC fluxes in the
146 Southern Ocean (Dunbar, 1984; Wefer et al., 1988; Wefer et al., 1990; Wefer and Fisher,
147 1991; Dubischar and Bathmann, 2002; Suzuki et al., 2001,2003; Accornero and Gowing,
148 2003; Schnack-Schiel and Isla, 2005; Gleiber et al., 2012) with a particular emphasis on shelf
149 ~~processes environments~~ where faecal pellet contribution to POC flux ~~is was~~ typically higher
150 than in the oceanic regions (Wefer et al., 1990; Wefer and Fischer, 1991; Schnack-Schiel and
151 Isla, 2005). In the Ross Sea there ~~is was~~ a northward decreasing contribution to carbon flux of
152 59 %, 38 % and 15 % for southern, central and northern areas reported from 235 m sediment
153 traps deployments (Schnack-Schiel and Isla, 2005). Faecal pellets in the Ross Sea ~~are were~~
154 generally represented by larger shapes with only 2 to 3 % of them present as small spherical
155 or ellipsoid shapes and total faecal pellet flux ~~is was~~ slightly higher than 10^3 pellet $m^{-2} d^{-1}$.
156 High faecal pellet contribution to carbon fluxes (> 90 %) ~~has have~~ been observed in the
157 Bransfield Strait and the Marginal Ice Zone of the Scotia Sea, and ~~have been~~ linked to the
158 abundance of the Antarctic krill *Euphausia superba*, resulting in maximum recorded fluxes of
159 $>5 \times 10^5$ pellets $m^{-2} d^{-1}$ (Bodungen, 1986; von Bodungen et al., 1987; Wefer et al., 1988). The
160 strong contribution of krill faecal pellets to carbon flux in the western Antarctic Peninsula was
161 confirmed over several years of observations, with the highest contributions to carbon flux
162 succeeding the phytoplankton bloom in January and February (Gleiber et al., 2012).

163 In the present study, particulate material exported from the mixed layer in the naturally
164 fertilized Permanently Open Ocean Zone (POOZ) of the Kerguelen Plateau is described from
165 an annual sediment trap mooring. To develop our understanding of seasonal variability in the
166 ecological flux vectors and particle biogeochemistry we investigate the link between the
167 chemical (POC, PON, BSi) and biological (diatom species and faecal pellet types)
168 components of exported particles. Furthermore, we advance the limitations of previous studies

169 by explicitly distinguishing full and empty diatom cells in the exported material and thereby
170 determine species-specific roles for carbon and silica export.

171 **2 Materials and methods**

172 As part of the multidisciplinary research program KEOPS2 a moored sediment trap
173 (Technicap PPS3) was deployed at 289 m (seafloor depth: 527 m) at the representative bloom
174 station A3 (50°38.3' S – 72°02.6' E) for a period of 321 days (21 October 2011 to 7
175 September 2012). The sediment trap mooring was located within an iron-fertilized bloom site
176 on the southern part of the Kerguelen Plateau (Blain et al., 2007). The cup rotation dates of
177 the sediment trap are listed in Table 1. Details of sediment trap design, hydrological
178 conditions, ~~deployment conditions~~ sample processing, ~~POC and PON analyses and surface~~
179 ~~chlorophyll *a* data extraction~~ are described in a companion paper (Rembauville et al., 2014).
180 ~~Comparison with thorium-based estimates of carbon export suggests a trapping efficiency of~~
181 ~~15-30 % relative to the proxy, although strong particle flux attenuation between 200 m and~~
182 ~~the trap depth (289 m) might also contribute to the low fluxes. We, therefore, interpret our~~
183 ~~results to accurately reflect the relationships between the biological and geochemical signals~~
184 ~~of the material caught by the sediment trap, which we acknowledge may not necessarily~~
185 ~~represent the entire particle export at 289 m.~~

186 ~~**2.1 Sediment trap sample processing**~~

187 ~~Details of sediment trap sample retrieval and processing methods have been presented in~~
188 ~~Rembauville et al. (this issue). In brief, swimmers were removed and classified from samples~~
189 ~~under a dissecting microscope. The samples were quantitatively divided into 8 aliquots using~~
190 ~~a Jencons peristaltic splitter with a precision of ~2.9 %. Particulate material was separated~~
191 ~~from the overlying preservative fluid by a centrifugation and freeze-drying procedure.~~

192 ~~**2.2 Chemical measurements**~~

193 ~~POC and PON analyses have been previously described in Rembauville et al. (this issue). In~~
194 ~~summary, 3 to 5 mg of freeze dried material were weighed directly into pre-combusted~~
195 ~~(450°C, 24h) silver cups and decarbonated through the addition of 2N HCl. Samples were~~
196 ~~dried overnight at 50 °C and POC and PON were measured with a CHN analyzer (Perkin~~
197 ~~Elmer 2400 Series II CHNS/O Elemental Analyzer) calibrated with glycine. Samples were~~
198 ~~analyzed in triplicate with an analytical precision of less than 0.3%.~~

199

200 **2.1 Biogenic and lithogenic silicon analyses.**

201 For the analysis of biogenic silica (BSi) and lithogenic silica (LSi), 2 to 8 mg of freeze-dried
202 material were weighed (Sartorius precision balance, precision 10^{-4} g) and placed into falcon
203 tubes. The extraction of silicon from biogenic and lithogenic particle phases was performed
204 following the Ragueneau et al. (2005) triple NaOH/HF extraction procedure. Silicic acid
205 ($\text{Si}(\text{OH})_4$) resulting from NaOH extractions was measured automatically on a Skalar 5100
206 autoanalyzer whereas $\text{Si}(\text{OH})_4$ resulting from HF extraction was measured manually on a
207 Milton Roy Spectronic 401 spectrophotometer. $\text{Si}(\text{OH})_4$ acid analyses were performed
208 colorimetrically following Aminot and Kerouel (2007). Standards for the analysis of samples
209 from the HF extraction were prepared in an HF/ H_3BO_4 matrix, ensuring the use of an
210 appropriate calibration factor that differs from Milli-Q water. The contribution of LSi to the
211 first leaching was determined by using Si:Al ratios from a second leaching step (Ragueneau et
212 al., 2005). Aluminum concentrations were measured by spectrophotometry (Howard et al.,
213 1986). The triple extraction procedure is **designed optimized** for samples with a BSi content <
214 10 μmol . For some samples (cup #3, #4, #6, #7, #8, #9 and #10) the Si:Al molar ratio in the
215 second leachate was high (>10) indicating the incomplete dissolution of BSi. For these
216 samples it was not possible to use Si:Al ratios to correct for LSi leaching. A crustal Si:Al
217 mass ratio of 3.74 (Taylor and McClennan, 1986) was **therefore** used **instead** and applied to

218 all the samples for consistency. Precision (estimated from measurement of 25 independent
219 samples) was 13 nmol/mg, which represents <1 % of the BSi content in all samples and 14 %
220 of the mean LSi content. Blank triplicates from each extraction were ~~lower than~~ below the
221 detection limit. BSi results from this method were compared to the kinetic method from
222 DeMaster (1981). There was an excellent agreement between the two methods (Spearman
223 rank correlation, $n = 12$, $p < 0.001$, $BSi_{\text{kinetic}} = 1.03 BSi_{\text{triple extraction}} - 0.08$, data not shown). To
224 estimate the contribution of opal to total mass flux, we assumed an opal composition of SiO_2
225 $0.4H_2O$ (Mortlock and Froelich, 1989).

226 In order to correct for the dissolution of BSi during deployment and storage, $Si(OH)_4$
227 excess was analyzed in the overlying preservative solution. Particulate BSi fluxes were
228 corrected for dissolution assuming that excess silicic acid originated only from the dissolution
229 of BSi phases. $Si(OH)_4$ excess was always <10 % of total (dissolved + particulate) Si
230 concentrations. Error propagation for POC, PON, BSi fluxes and molar ratios were calculated
231 as the quadratic sum of the relative error from triplicate measurements of each variable.

232 **2.2 Diatom identification, fluxes and biomass**

233 Many sediment trap studies reporting diatom fluxes in the Southern Ocean use a
234 micropaleontological protocol that oxidizes organic material ($KMnO_4$, HCl , H_2O_2) thereby
235 facilitating the observation of diatom ~~frustules~~ valves (see Romero et al., 1999, 2000 for a
236 description). In the present manuscript, our specific aim was to separately enumerate full and
237 empty diatom cells captured by the sediment trap to identify key carbon or silicon exporters
238 amongst the diatom species. We therefore used a biological method following a similar
239 protocol to that of (Salter et al., 2007, 2012). To prepare samples for counting, 2 mL of a
240 gently homogenized 1/8 wet aliquot were diluted in a total volume of 20 mL of artificial
241 seawater ($S = 34$). In order to minimize the exclusion and/or breaking of large or elongated
242 diatom frustules (e.g. *Thalassiothrix antarctica*), the pipette tip used for sub-sampling was

243 modified to increase the tip aperture to >2 mm. The diluted and homogenized sample was
244 placed in a Sedgewick-Rafter counting chamber (Pyser SGE S52, 1 mL chamber volume).
245 Each sample was observed under an inverted microscope (Olympus IX71) with phase contrast
246 at 200x and 400x magnification. Diatom enumeration and identification was made from one
247 quarter to one half of the counting chamber (depending on cell abundance). **The total number**
248 **of diatoms counted was >400 in all the cups with exception to the winter cup #12 (May –**
249 **September 2012) where the diatom abundance was low (<100 diatoms counted).** Diatoms
250 species were identified following the ~~taxonomic description in~~ recommendations of Hasle and
251 Syvertsen (1997). **All whole, intact and recognizable frustules were enumerated. Full and**
252 **empty cells were counted separately, following suggestions in Assmy et al. (2013).**

253 Due to the lower magnification used and preserved cell contents sometimes obscuring
254 taxonomic features on the valve face, taxonomic identification to the species level was
255 occasionally difficult and necessitated the categorizing of diatom species to genus or taxa
256 groupings in the following manner: *Chaetoceros* species of the subgenus *Hyalochaete* resting
257 spores (CRS) were not differentiated into species or morphotypes but were counted separately
258 from the vegetative cells; *Fragilariopsis separanda* and *Fragilarsiopsis rhombica* were
259 grouped as *Fragilariopsis separanda/rhombica*; *Membraneis imposter* and *Membraneis*
260 *challengeri* and species of the genera *Banquisia* and *Manguinea* were denominated as
261 *Membraneis* spp. (Armand et al., 2008a); diatoms of the genus *Haslea* and *Pleurosigma* were
262 grouped as *Pleurosigma* spp.; all *Pseudo-nitzschia* species encountered were grouped as
263 *Pseudo-nitzschia* spp.; *Rhizosolenia antennata* and *Rhizosolenia styliiformis* were grouped as
264 ~~*Rhizosolenia—antenanta/styliiformis*~~ *Rhizosolenia antennata/styliiformis*; large and rare
265 *Thalassiosira oliverana* and *Thalassiosira tumida* were grouped as *Thalassiosira* spp.;
266 *Thalassiosira antarctica* resting spores (TRS) were identified separately from the vegetative
267 cells; small centric diatoms (<20 µm) represented by *Thalassiosira gracilis* and other

268 *Thalassiosira* species were designated as Small centrics (< 20µm); and finally large and rare
269 centrics including *Azpeitia tabularis*, *Coscinodiscus* spp. and *Actinocyclus curvatulus* were
270 grouped as Large centrics (>20 µm). Full and empty frustules of each species or taxa grouping
271 were distinguished and enumerated separately. The cell flux for each diatom species or taxa
272 grouping was calculated according to Equation (1):

$$273 \quad Cell\ flux = N_{diat} \times d \times 8 \times V_{cup} \times \frac{1}{0.125} \times \frac{1}{days} \times chamber\ fraction \quad (1)$$

274 Where *Cell flux* is in valves m⁻² d⁻¹, *N_{diat}* is the number of cells enumerated for each diatom
275 classification, *d* is the dilution factor from the original wet aliquot, 8 is the total number of
276 wet aliquots comprising one sample cup, *V_{cup}* is the volume of each wet aliquot, 0.125 is the
277 Technicap PPS/3 sediment trap collecting area (m²), *days* is the collecting period, *chamber*
278 *fraction* is the surface fraction of the counting chamber that was observed (one quarter or one
279 half). The annually integrated full and empty diatom flux for each species was calculated
280 assuming as follows:

$$281 \quad Annual\ flux_{(x)} = \sum_{i=1}^{12} (Flux_{(x)i} \times days_i) \quad (2)$$

282
283
284 Where *Annual flux_(x)* is the annually integrated flux of a full or empty diatom species *x* (cell
285 m⁻² y⁻¹), *Flux_{(x)i}* is the full or empty flux of this species in the cup number *i* (cell m⁻² d⁻¹) and
286 *days_i* is the collecting time for the cup number *i* (d). The calculations assume negligible export
287 occurred during the month of September which was not sampled by the sediment trap. We
288 consider this assumption reasonable based on the preceding flux profile and low concentration
289 of satellite-derived chlorophyll (Rembauville et al. 2014).

290

291 We directly compared the micropaleontological (as used in Rigual-Hernández et al.
292 (2015)) and biological counting techniques in our sediment trap samples and noted the loss of
293 several species (*Chaetoceros decipiens*, *Chaetoceros dichaeta*, *Corethron pennatum*
294 *Corethron inerme*, *Guinardia cylindrus* and *Rhizosolenia chunii*) under the
295 micropaleontological technique. We attribute this to the aggressive chemical oxidation
296 techniques used to “clean” the samples as well as the centrifugation steps which may also
297 selectively destroy or dissolve certain frustules. For the species that were commonly observed
298 by both techniques, total valve flux was in good agreement (Spearman rank correlation, $n =$
299 12 , $\rho = 0.91$, $p < 0.001$, data not shown) although consistently lower with the
300 micropaleontological technique, probably due to the loss of certain frustules described above.
301 Full details of this method comparison are in preparation for a separate submission.

302 Diatoms species that contributed to more than 1 % of total full cell flux were
303 converted to carbon flux. For *E. antarctica* var. *antarctica*, *Fragilariopsis kerguelensis*,
304 *Fragilariopsis separanda/rhombica*, *Pseudo-nitzschia* spp. and *Thalassionema nitzschioides*
305 spp., we used published cell-specific carbon content ($Cell_C$, pgC cell^{-1}) for diatoms
306 communities of the Kerguelen Plateau from Cornet-Barthaux et al. (2007). As *Chaetoceros*
307 *Hyalochaete* resting spores (CRS) and *Thalassiosira antarctica* resting spores (TRS) largely
308 dominated the full diatom fluxes (>80%), an appropriate estimation of their carbon content
309 based on the specific sizes observed in our dataset was required for accurate quantification of
310 their contribution to carbon fluxes. Biomass calculations for both CRS and TRS were
311 determined from >50 randomly selected complete resting spores observed in splits from cups
312 #4 to #11 (December 2011 to May 2012). Morphometric measurements (pervalvar and apical
313 axis) were made using the Fiji image processing package (available at <http://fiji.sc/Fiji>) on
314 images taken with an Olympus DP71 camera. Cell volumes followed appropriate shape
315 designated calculations from Hillebrand et al. (1999) (Table 2). The cell volume coefficient of

316 variation was 46 % and 54 % for CRS and TRS, respectively. CRS carbon content was
 317 estimated from the derived cell volume using the volume to carbon relationship of 0.039
 318 pmolC μm^{-3} established from the resting spore of *Chaetoceros pseudocurvisetus* (Kuwata et
 319 al., 1993), leading to a mean $Cell_C$ value of 227 pgC cell⁻¹ (Table 2). There is currently no
 320 volume to carbon relationship for *Thalassiosira antarctica* resting spores described in the
 321 literature, therefore, the allometric relationship for vegetative diatoms (Menden-Deuer and
 322 Lessard, 2000) was used to calculate our TRS carbon content, giving a mean $Cell_C$ value of
 323 1428 pgC cell⁻¹ (Table 2). Full diatom fluxes were converted to carbon fluxes as follows:

$$324 \quad C \text{ flux}_{(x)} = \frac{Flux_{(x)} \times Cell_{C(x)}}{M_{12C} \times 10^9} \quad (3)$$

325 where $C \text{ flux}_{(x)}$ is the carbon flux carried by each diatom species x (mmol C m⁻² d⁻¹), $Flux_{(x)}$ is
 326 the full cell numerical flux of species x (cell m⁻² d⁻¹), $Cell_{C(x)}$ is the carbon content of species x
 327 (pgC cell⁻¹) and M_{12C} is the molecular weight of ¹²C (12 g mol⁻¹) and 10^9 is a conversion factor
 328 from pmol to mmol. ~~Other diatoms species that contributed to more than 1 % of total cell flux~~
 329 ~~(*E. antarctica* var. *antarctica*, *Fragilariopsis kerguelensis*, *Fragilariopsis*~~
 330 ~~*separanda/rhombica*, *Pseudo-nitzschia* spp. and *Thalassionema nitzschioides* spp.) were~~
 331 ~~converted to carbon flux using cell-specific carbon content for diatoms communities of the~~
 332 ~~Kerguelen Plateau from Cornet-Barthaux et al. (2007).~~

333 **2.3 Faecal pellet composition and fluxes**

334 To enumerate faecal pellets an entire 1/8 aliquot of each sample cup was placed in a gridded
 335 petri dish and observed under a stereomicroscope (Zeiss Discovery V20) coupled to a camera
 336 (Zeiss Axiocam ERc5s) at 10x magnification. Photographic images (2560 x 1920 pixels, 3.49
 337 $\mu\text{m pixel}^{-1}$) covering the entire surface of the petri dish were acquired. Following Wilson et al.
 338 (2013), faecal pellets were classified into five types according to their shape: spherical, ovoid,

339 cylindrical, ellipsoid and tabular. The flux of each faecal pellet class ($\text{nb m}^{-2} \text{d}^{-1}$) was
340 calculated as follows:

$$341 \quad \text{Faecal pellet flux} = N_{FP} \times 8 \times \frac{1}{0.125} \times \frac{1}{\text{days}} \quad (4)$$

342 where N_{FP} is the number of pellets within each class observed in the 1/8th aliquot. The other
343 constants are as described in Eq. (1). Individual measurements of the major and minor axis for
344 each faecal pellet were performed with the Fiji software. The total number of spherical, ovoid,
345 cylindrical, ellipsoid and tabular faecal pellets measured was 4041, 2047, 1338, 54 and 29,
346 respectively. Using these dimensions, faecal pellet volume was determined using the
347 appropriate shape equation (e.g. sphere, ellipse, cylinder, ovoid/ellipse) and converted to
348 carbon using a factor of 0.036 mgC mm^{-3} (Gonzalez and Smetacek, 1994). Due to the
349 irregularity of the tabular shapes preventing the use of single equation to calculate their
350 volume, a constant value of 119 $\mu\text{gC pellet}^{-1}$ representing a midrange value for tabular shapes
351 (Madin, 1982), was applied to tabular faecal pellets (Wilson et al., 2013). This value was
352 ~~relevant~~ appropriate because the observed tabular faecal pellets were ~~comprised-in~~ within the
353 size range reported in Madin (1982). Ranges and mean values of faecal pellet volumes and
354 carbon content are reported in Table 3. Faecal fluff and disaggregated faecal pellets were not
355 considered in these calculations because quantitative determination of their volume is
356 difficult. We acknowledge that fragmentation of larger pellets may represent an artifact of the
357 sample splitting procedure. Alternatively, their presence may also result from natural
358 processes within the water column, although dedicated sampling techniques (e.g.
359 polyacrylamide gel traps) are required to make this distinction (Ebersbach et al., 2014, 2011;
360 Ebersbach and Trull, 2008; Laurenceau et al., 2014). Consequently our present quantification
361 of faecal pellet carbon flux should be considered as lower-end estimates.

362 The precision of our calculations depends on the reliability of carbon-volume
363 conversion factors of faecal pellets, which vary widely in the literature, as well as variability
364 in diatom resting spore volumes (Table 2). To constrain the importance of this variability on
365 our quantitative estimation of C flux, we calculated upper and lower error bounds by a
366 constant scaling of the conversion factors ($\pm 50\%$).

367 **2.4 Statistical analyses**

368 Correspondence analysis was performed to summarize the seasonality of diatom export
369 assemblages. This approach projects the original variables (here full and empty cells) onto a
370 few principal axes that concentrate the information of the Chi-squared (χ^2) distance
371 between both observations and variables (Legendre and Legendre, 1998). χ^2 distance is
372 very sensitive to rare events. ~~Consequently, only full and empty cells fluxes >10% of the~~
373 ~~total mean flux of all sample cups were retained in the correspondence analysis. This step~~
374 ~~avoided the inclusion of rare species, which potentially carry a lot of weight in the analysis~~
375 ~~despite providing weak information.~~ Consequently, only species with an annual mean flux
376 higher than 10% of the mean annually integrated flux of all the species were retained in the
377 correspondence analysis. This selection was performed separately on full and empty cell
378 fluxes.

379 Partial least square regression (PLSR) analysis was used to examine the relationships
380 between ecological flux vectors (full and empty diatom cells and faecal pellet fluxes as
381 columns of the X matrix, cups being the rows) and bulk geochemical properties (POC flux,
382 PON flux, BSi flux, POC:PON and BSi:POC molar ratio and columns in the Y matrix) of the
383 exported material. The principle of PLSR is to decompose both the X and Y matrix into their
384 principal components using principal component analysis and then use these principal
385 components to regress Y in X (Abdi, 2010). PLSR is capable of modeling response variables

386 from a large set of predictors. The same filter as for the correspondence analysis (full- and
387 empty -cell fluxes >10 % of the total mean flux) was applied.

388 **3 Results**

389 **3.1 Chemical composition of the settling material**

390 Time series of the chemical signature of the settling material are presented in Fig. 1
391 and export fluxes are reported in Table 1. POC and PON fluxes are already reported and
392 discussed in the companion paper (Rembauville et al., 2014). ~~Surface chlorophyll *a*~~
393 ~~concentration above the trap location and POC fluxes (Fig. 1a and 1b) have been described~~
394 ~~and discussed in Rembauville et al. (2014). Elemental fluxes are reported in Table 1. POC~~
395 ~~fluxes were low most of the time ($\leq 0.5 \text{ mmol m}^{-2} \text{ d}^{-1}$) except during two short and intense~~
396 ~~export events in early December ($1.6 \text{ mmol m}^{-2} \text{ d}^{-1}$) and late January early February (1.47~~
397 ~~$\text{mmol m}^{-2} \text{ d}^{-1}$). Assuming a negligible flux during the unsampled period (the month in~~
398 ~~September), the annual POC export was $98.2 \pm 4.3 \text{ mmol m}^{-2}$ (total \pm sum of time integrated~~
399 ~~standard deviations). BSi fluxes exhibited the same seasonal pattern than as POC fluxes (Fig.~~
400 1c) with low fluxes ($< 1 \text{ mmol m}^{-2} \text{ d}^{-1}$) except during the two intense events (2.60 ± 0.03 and
401 $2.19 \pm 0.10 \text{ mmol m}^{-2} \text{ d}^{-1}$, mean \pm standard deviation). LSi fluxes were highest in in spring
402 ($>10 \mu\text{mol m}^{-2} \text{ d}^{-1}$ in cups #1 to #4, **October to December 2011**, Table 1). The contribution of
403 LSi to total particulate Si was 5 % and 10 % respectively in cups #1 (**October/November**
404 **2011**) and #12 (**May to September 2012**) and lower than 3 % the remainder of the year. ~~The~~
405 ~~POC:PON molar ratio showed low variability, ranging between 6 and 8.1, with a maximum~~
406 ~~value observed in autumn (cup #11). The BSi:POC molar ratio was highest at the beginning~~
407 of the season (between 2.18 ± 0.19 and 3.46 ± 0.16 in the first three cups **from October to**
408 **December 2011**, blue line in Fig. 1c) and dropped to 0.64 ± 0.06 in cup #5 (**end December**
409 **2011**), following the first export event. BSi:POC ratios were close in the two export events

410 (1.62 ± 0.05 and 1.49 ± 0.08). The lowest BSi:POC ratio was observed in autumn in cup #11
411 (0.29 ± 0.01, February to May 2012). Similarly, the opal contribution to total mass flux was
412 highest in spring (70.8 % in cup #2, November 2011) and lowest in autumn (21.5 % in cup
413 #11, February to May 2012).

414 3.2 Diatom fluxes

415 Diatoms from 33 taxa were identified and their fluxes determined across the 11-months time
416 series. Fluxes are reported in Table 4 and Table 5 for full and empty cells, respectively. Full
417 and empty cell fluxes for the total community and for the taxa that are the major contributors
418 to total diatom flux (eight taxa that account for >1 % of total cells annual export) are
419 presented in Fig. 2. The ~~flux-of~~ full- and empty-cell fluxes for each diatom species or taxa is
420 reported in Table 4.

421 During spring (cups #1 to #3, October to December 2011) and autumn/winter (cups
422 #11 and #12, February to September 2012) the total flux of full cells was $< 5 \times 10^6$ cells $m^{-2} d^{-1}$
423 (Fig. 2a). The total flux of full cells increased to 5.5 and 9.5×10^7 cells $m^{-2} d^{-1}$ (cups #4 and
424 #9, December and end January respectively) during two episodic (<14 days) sedimentation
425 events. The two largest flux events (cups #4 and #9) were also associated with significant
426 export of empty cells with respectively 6.1×10^7 and 2.9×10^7 cells $m^{-2} d^{-1}$ (Fig. 2a). For
427 *Chaetoceros Hyalochaete* spp. resting spores (CRS), full cells fluxes of 4×10^7 cells $m^{-2} d^{-1}$
428 and 7.8×10^7 cells $m^{-2} d^{-1}$ accounted for 76 % and 83 % of the total full cell flux during these
429 two events, respectively (Fig. 2b), whereas a smaller contribution of *Thalassiosira antarctica*
430 resting spores (TRS) (2.7×10^6 cells $m^{-2} d^{-1}$, 5 % of total full cells) was observed during the
431 first event (Fig. 2h). CRS also dominated (79-94 %) the composition of full cells in the
432 intervening period (cups #5-#8, December 2011 to January 2012), although the magnitude of
433 cell flux was moderate ($9 \times 10^6 - 2.5 \times 10^7$ cells $m^{-2} d^{-1}$) by comparison (Fig. 2b). In cup #4

434 (December 2011), the empty cell flux contained 61 % of *C. Hyalochaete* spp. vegetative
435 empty cells and 27 % of unidentified Small centrics (<20 µm) empty cells. In cup #9 (end
436 January 2012), the total empty cells flux contained 60 % of *C. Hyalochaete* spp. vegetative
437 stage and only 2 % of Small centrics (<20 µm) empty cells.

438 *Fragilariopsis kerguelensis*, and *Fragilariopsis separanda/rhombica* (Fig. 2d and 2e)
439 were mostly exported from spring through the end of summer (cups #1 to #10, October 2011
440 to February 2012) with total (full + empty) fluxes $< 3 \times 10^6$ cells $m^{-2} d^{-1}$, a value ~20 times
441 lower than the highest CRS fluxes recorded. During this time, these species were represented
442 by >50 % of empty cells. In autumn and winter, (cups #10 and #11, February to May 2012),
443 these species were only represented by low fluxes ($< 0.5 \times 10^6$ cells $m^{-2} d^{-1}$) of empty cells.
444 *Thalassionema nitzschioides* spp. fluxes were highest in spring and early summer (cups #1 to
445 #4, October to December 2011) with total fluxes comprised between 3.5×10^6 and 6.7×10^6
446 cells $m^{-2} d^{-1}$ (Fig. 2g). The remainder of the year, total flux was $< 2 \times 10^6$ cells $m^{-2} d^{-1}$ and was
447 essentially represented by full cells. *Pseudo-nitzschia* spp. were mostly represented by full
448 cells (Fig. 2f) with the highest flux of 1.2×10^7 cells $m^{-2} d^{-1}$ observed in the second intense
449 export event (cup #9, end January 2012). *Eucampia antarctica* var. *antarctica* total fluxes
450 were always represented by >50 % of full cells (Fig. 2c). Total cell fluxes of *Eucampia*
451 *antarctica* var. *antarctica* gradually increased from $< 1 \times 10^5$ to 1.3×10^6 cells $m^{-2} d^{-1}$ from
452 spring to summer (cups #1 to #9, October 2011 to January 2012) and then decreased to a
453 negligible flux in winter (cup #12, May to September 2012). This species was observed as
454 both the lightly silicified, chain-forming, vegetative form and the highly silicified winter
455 growth stage form. Both forms were observed throughout the year without specific seasonal
456 pattern. Small centric species (<20 µm) were essentially represented by empty cells (Fig. 2i).
457 Their total fluxes were $< 4 \times 10^6$ cells $m^{-2} d^{-1}$, except in the first export event (cup #4,
458 December 2011) where their flux represented a considerable export of 1.7×10^7 cells $m^{-2} d^{-1}$.

459 Diatoms and sampling cup projection on the first two axes from the correspondence
460 analysis is presented in Fig. 3. Chi² distance in the correspondence analysis is based on
461 frequency distribution, therefore the results of the analysis must be considered as
462 representative of the community composition as opposed to cell flux. The first two factors
463 accounted for the majority (75.6 %) of total explained variance. Early in the season (cups #1-
464 #3, **October to mid-December 2011**), during the period of biomass accumulation in the
465 surface (Fig 1a), diatom fluxes were characterized by empty cells of *T. nitzschioides* spp. and
466 *F. kerguelensis*. Full TRS cells were observed in cup #3 (**end November 2011**) following the
467 initial bloom decline. The first major flux event (cup #4, **December 2011**) contained mostly
468 TRS, empty Small centrics (< 20 µm) cells and empty *C. Hyalochaete* spp. cells. The summer
469 flux period (cups #5 to #8, **December 2011 to January 2012**) primarily consisted of CRS,
470 although *E. antarctica* var. *antarctica*, *Pseudo-nitzschia* spp, and *Thalassiothrix antarctica*
471 were present as full cells and *Plagiotropis* spp., *Membraneis* spp., *Pseudo-nitzschia* spp. as
472 empty cells. The second major flux event (cup #9, **end January 2012**) was tightly associated
473 with CRS and full *Pseudo-nitzschia* spp. cells. Subsequent cups (#10 and #11, **February to**
474 **May 2012**) were characterized by full cells of *E. antarctica* var. *antarctica* and *Thalassiothrix*
475 *antarctica* and empty cells of *Corethron inerme*, *P. alata*, *F. separanda/rhombica* and *F.*
476 *kerguelensis*. Winter fluxes (cup #12, **May to September 2012**) were similar to the initial three
477 cups characterized primarily by empty cells of small diatom taxa. The centralized projection
478 in Fig. 3 of full *F. kerguelensis* and *T. nitzschioides* spp. highlights their constant presence
479 throughout the annual record.

480 The total empty:full cell ratio is presented in Fig. 2a (blue line). This ratio was highest
481 in spring and early summer (cups #1 to #4, **October to December 2011**), ranging between 1.1
482 and 2.4, suggesting more empty cells to full cells. The ratio was lowest, representing
483 considerably more full cells to empty cells in cups #5 to #10 (**December 2011 to February**

484 2012) with values between 0.1 and 0.4. In autumn (cup #11, February to May 2012), the
485 empty:full ratio increased to 0.7. In the winter cup #12 (May to September 2012), the total
486 amount of full diatom cells was very low and therefore we could not calculate a robust
487 empty:full ratio. Across the time-series certain diatom taxa were observed exclusively as
488 empty cells, notably *Chaetoceros atlanticus* f. *bulbosum*, and *Corethron pennatum*. For
489 diatom taxa present as full and empty cells we calculated an annually integrated empty:full
490 ratio (Fig. 4) and arbitrarily defined threshold values of 2 (representing species mainly
491 observed as empty cells) and 0.5 (representing species mainly observed as full cells),
492 respectively. In decreasing order, the diatom taxa exhibiting empty:full ratios >2 were
493 *Thalassiosira lentiginosa*, Small centrics (< 20µm), *Proboscia alata*, *Rhizosolenia*
494 *antennata/styliformis*, *Chaetoceros decipiens*, *Corethron inerme*, *Dactyliosolen antarcticus*,
495 Large centrics (> 20 µm), and *Asteromphalus* spp. The diatom taxa displaying an empty:full
496 ratio <0.5 were *Thalassiothrix antarctica*, *Rhizosolenia simplex*, CRS, *Eucampia antarctica*
497 var. *antarctica*, *Thalassiosira* spp. and *Navicula* spp. Species or grouped taxa with ratio
498 values falling between the thresholds (<2 and >0.5; *R. chunii*, through to *C. dichæta* in Fig.
499 4) were perceived as being almost equally represented by full and empty cells when integrated
500 annually across the time series.

501 3.3 Faecal pellet fluxes

502 The seasonal flux of faecal pellet type, volume and their estimated carbon flux are
503 summarized in Fig. 5 and Table 6. Total faecal pellet flux was $<2 \times 10^3$ pellets $m^{-2} d^{-1}$ in
504 spring (cups #1 to #3, October to December 2011). Cups #4 and #5 (December 2011) were
505 characterized by the highest fluxes of 21.8×10^3 and 5.1×10^3 pellets $m^{-2} d^{-1}$ (Fig. 5a, Table
506 6). Faecal pellet numerical flux decreased gradually from mid-summer (cup# 5, December
507 2011) to reach a minimal value in winter (140 pellets $m^{-2} d^{-1}$ in cup #12, May to September
508 2012). In spring (cups #1 to #3, October to December 2011), spherical and cylindrical shapes

509 dominated the numerical faecal pellet fluxes. Ellipsoid and tabular shapes were absent from
510 these spring cups. The first export event (cup #4, **December 2011**), was numerically
511 dominated by the spherical shaped pellets, however the remainder of the summer (cups #5 to
512 #10, **December 2011 to February 2012**) contained spherical, ovoid and cylindrical shapes in
513 comparable proportions. Ellipsoid shapes were observed from mid-summer to autumn (cups
514 #7 to #11, **January to May 2012**) but their overall contribution to pellet flux was low (<6 %,
515 Table 6). Rare tabular shapes were observed in summer (cups #6 and #8, **December and**
516 **January 2012**) and their contribution to numerical fluxes was highest in autumn and winter
517 (cups #11 and #12, **February to September 2012**).

518 The median faecal pellet volume showed a seasonal signal with a maximum peak >
519 $5.5 \times 10^6 \mu\text{m}^3$ in mid-summer (cups # 6 to #8, **mid-December to January 2012**) and values <4
520 $\times 10^6 \mu\text{m}^3$ the remainder of the year (Fig. 5b). Concomitantly with the highest median
521 volume, the largest variance in faecal pellet size was also observed in the summer (highest
522 interquartile values in Fig. 5b).

523 Total faecal pellet carbon flux was lowest in spring (< 0.05 mmolC m⁻² d⁻¹ in cups #1
524 to #3, **October to December 2011**, Fig. 5c, Table 6). The highest total faecal pellet carbon flux
525 of nearly 0.5 mmolC m⁻² d⁻¹ was observed during the first export event in cup #4 (**December**
526 **2011**) and was essentially composed of spherical shapes (83 %, Table 6). For the remainder of
527 the summer (cups #5 to #10, **December 2011 to February 2012**), total faecal pellet carbon flux
528 was between 0.03 and 0.15 mmolC m⁻² d⁻¹ with a dominant contribution of cylindrical,
529 ellipsoid and tabular shapes. In autumn and winter (cups #11 and #12, **February to September**
530 **2012**), faecal pellet carbon fluxes of 0.13 and 0.06 mmolC m⁻² d⁻¹ were strictly dominated by
531 tabular shapes (> 90 % to total faecal pellet carbon fluxes, Table 6).

532 **3.4 Statistical analysis of biological and biogeochemical signatures**

533 The β correlation coefficients of standardized variables obtained from the PLSR
534 analysis are presented as a heatmap in Fig. 6. The full cell fluxes of all diatom taxa, in
535 addition to spherical and ovoid and ellipsoid faecal pellet fluxes were positively correlated to
536 POC and PON fluxes. By contrast, empty cell fluxes of *F. kerguelensis*, *P. alata*, *T.*
537 *nitzschioides* spp., *T. lentiginosa* and cylindrical, ellipsoid and tabular pellet fluxes were
538 either uncorrelated or negatively correlated with POC and PON fluxes. Full- and empty-cell
539 fluxes of all diatom taxa were positively correlated with BSi fluxes, although this correlation
540 was notably weak for empty cells of *C. inerme*, *P. alata* and *T. lentiginosa*. Only spherical
541 and ovoid faecal pellets were positively correlated with BSi fluxes. Full cells fluxes of CRS
542 and *E. antarctica* var. *antarctica* were the most negatively correlated with BSi:POC molar
543 ratio, whereas TRS, *F. kerguelensis*, *T. nitzschioides* spp. and *T. lentiginosa* full cells fluxes
544 were positively correlated. Spherical and ovoid faecal pellets were weakly and negatively
545 correlated with the BSi:POC molar ratio whereas the cylindrical, ellipsoid and tabular shapes
546 were more strongly negatively correlated to the BSi:POC molar ratio. All the biological
547 components exhibited weak or no correlations to the POC:PON molar ratio.

548 The first two latent vectors of the PLSR accounted for 61.3 % and 74.1 % of
549 cumulative variance in X (full and empty diatom and pellet fluxes) and Y (biogeochemical
550 properties). In order to visualize how the seasonal succession of flux vectors was related to
551 the bulk geochemical properties of particles, the sampling cups, biological and chemical
552 factors were projected on the first two latent factors of the PLSR analysis (Fig. 7). (Fig. 8).
553 Positively projected on the first axis are the POC, PON and BSi fluxes, close to the export
554 events sampled in cups #4 (December 2011) and #9 (end January 2012). The closest
555 biological components comprise a complex assemblage of full and empty cells and spherical
556 and ovoid faecal pellet shapes. All the other cups are projected far from these two export
557 events. The second axis opposes the spring cups (#1 to #3, October to mid-December 2011) to

558 the autumn (#11, February to May 2012) and winter (#12, May to September 2012) cups.
559 Empty frustules of *F. kerguelensis*, *T. lentiginosa* and *T. nitzschioides* spp. are projected close
560 to the spring cups (#1 to #3, October to mid-December 2011) together with the BSi:POC
561 molar ratio whereas autumn (#11, February to May 2012) and winter cups (#12, May to
562 September 2012) are projected far from the BSi:POC molar ratio and close to the tabular and
563 cylindrical faecal pellet shapes.

564 3.5 Partitioning carbon fluxes among ecological vectors

565 We estimated the contribution of resting spores and faecal pellets to carbon flux, calculated
566 their cumulative values and compared them to measured values (Fig. 8a and 8b). A highly
567 significant correlation (Spearman rank correlation, $n = 36$, $\rho = 0.84$, $p < 0.001$) was evident
568 between calculated and measured carbon flux suggesting that the main ecological flux vectors
569 observed in the sample were capable of explaining the seasonal variation in total POC flux.
570 Table 7 lists the contribution of each vector to the calculated flux. In cup #1 (October to mid-
571 November 2011), CRS and other diatoms dominated the calculated POC fluxes, with
572 respectively 25.3 % and 38.6 %. Diatoms other than spores dominated the calculated carbon
573 flux (35.4 %) together with cylindrical faecal pellets (36.4 %) in cup #2 (November 2011).
574 TRS dominated the POC fluxes (85.1 %) in cup #3 (November/December 2011) (85.1%).
575 CRS strictly dominated the calculated POC fluxes in summer (cups #4 to #10, December
576 2011 to February 2012) with a contribution ranging from 46.8 % to 88.1 %. During the
577 autumn and winter (cups #11 and #12, February to September 2012), POC fluxes were almost
578 exclusively associated to tabular faecal pellets, 81 % and 93.3 %, respectively. At annual
579 scale diatoms resting spores (CRS and TRS), other diatoms and faecal pellets respectively
580 accounted for 60.7 %, 5 % and 34.3 % of the calculated POC fluxes. Annual POC fluxes
581 estimated from ecological vectors considered here were slightly less than measured values
582 (93.1 versus 98.2 mmol m⁻²).

583 4 Discussion

584 4.1 The significance of resting spores for POC flux

585 ~~Although there was generally a strong attenuation of flux between the base of the winter~~
586 ~~mixed layer (WML) and 300 m on the Kerguelen Plateau (Rembauville et al 2014), we~~
587 ~~observed significant variability in export over the annual cycle.~~ In a companion paper we
588 present multiple lines of evidence that converge on a scenario of strong flux attenuation
589 between the base of the winter mixed layer (WML at ~220 m) and 300 m on the Kerguelen
590 Plateau (Rembauville et al., 2014). Most notably large attenuation coefficients (3.3 – 4) were
591 calculated from independent measurements in spring and summer. (Ebersbach and Trull, 2008;
592 Jouandet et al., 2014). Strong flux attenuation and under trapping due to hydrodynamics and
593 swimmers combine to explain the low annually-integrated POC fluxes. ~~However, we~~
594 ~~observed significant variability in export over the annual cycle.~~ Generally POC fluxes were
595 $<0.5 \text{ mmol m}^{-2} \text{ d}^{-1}$ with the notable exception of two pulsed (<14 days) export events of ~ 1.5
596 $\text{mmol m}^{-2} \text{ d}^{-1}$ that accounted for ~ 40 % of annual POC export. These two flux events were
597 characterized by a noticeable increase and general dominance of diatom resting spores.
598 During both of these pulsed export events, cumulative *Chaetoceros Hyalochaete* spp. resting
599 spores (CRS) and *Thalassiosira antarctica* resting spores (TRS) fluxes accounted for 66 %
600 and 88 % of the measured POC flux, whereas total faecal pellet flux accounted for 29 % and
601 5.2 %, respectively (Table 7). The combination of CRS and TRS were responsible for 60.7 %
602 of the annual calculated POC flux, a value ten times higher than the contribution of other
603 diatoms (5 %). We did not observe any full cells of the vegetative stage of *Chaetoceros*
604 *Hyalochaete*, a feature possibly related to its high susceptibility to grazing pressure in the
605 mixed layer (Smetacek et al., 2004; Quéguiner, 2013; Assmy et al., 2013). Empty
606 *Chaetoceros Hyalochaete* spp. cells were vegetative stages different in shape from the resting
607 spores. ~~It can be the remaining of~~ These empty frustules ~~may can~~ be the remnants of

608 vegetative stages following the spore formation. ~~formation or the result of the consumption of~~
609 ~~the organic material by grazing.~~ Alternatively, dissolution of the lightly silicified valves or
610 girdle bands of the vegetative cell could result in the rapid consumption of the cellular organic
611 material in the upper water column and this may also explain the absence of full vegetative
612 cells in the sediment trap record. Our flux data reveal that small (10 to 30 μm) and highly
613 silicified resting spores bypass the intense grazing pressure characterizing the base of the
614 mixed layer, and are the primary mechanism through which carbon and, to a lesser extent
615 silicon, is exported from the surface.

616 Numerous sediment trap studies have reported a strong contribution, if not dominance,
617 of CRS to diatom fluxes at depth in various oceanographic regions: firstly, in coastal
618 influenced regions (e.g. Antarctic Peninsula (Leventer, 1991), Bransfield Strait (Abelmann
619 and Gersonde, 1991), Gulf of California (Sancetta, 1995), the Omura Bay (Kato et al., 2003),
620 North Pacific Ocean (Chang et al., 2013) and the Arctic (Onodera et al., 2014)), secondly in
621 upwelling-influenced regions (e.g. Santa Barbara basin (Lange, 1997), Eastern Equatorial
622 Atlantic (Treppke et al., 1996)) and finally in the open ocean in the subarctic Atlantic
623 (Rynewson et al., 2013). Similar to sediment trap observations, CRS are reported as dominant
624 in surface sediments of coastal regions (peri-Antarctic shelf and Antarctic sea ice (Crosta et
625 al., 1997; Zielinski and Gersonde, 1997; Armand et al., 2005), the North Scotia Sea (Allen et
626 al., 2005) and east of Kerguelen Island (Armand et al., 2008b)), but also in upwelling-
627 influenced regions (the northeastern Pacific (Grimm et al., 1996), the northeast Pacific (Lopes
628 et al., 2006)) and finally in the open ocean (the North Atlantic, Bao et al., 2000). ~~(e.g.~~
629 ~~Antarctic Peninsula (Leventer, 1991), Bransfield Strait (Abelmann and Gersonde, 1991), Gulf~~
630 ~~of California (Sancetta, 1995; Lange et al., 1997), Eastern Equatorial Atlantic (Treppke et al.,~~
631 ~~1996), East China Sea the Omura Bay (Kato et al., 2003), coastal North Pacific Ocean (Chang~~
632 ~~et al., 2013) and the subarctic Atlantic (Rynewson et al., 2013) and the Arctic (Onodera et al.,~~

633 ~~2014)). CRS are also found to be dominant in surface sediments in the coastal northeastern~~
634 ~~Pacific (Grimm et al., 1996), the North Atlantic (Bao et al., 2000), the northeast Pacific~~
635 ~~(Lopes et al., 2006), the North Scotia Sea (Allen et al., 2005), Antarctic sea ice and coastal~~
636 ~~regions (Crosta et al., 1997; Zielinski and Gersonde, 1997; Armand et al., 2005), and east of~~
637 ~~Kerguelen Island (Armand et al., 2008b).~~ Moreover, the annual POC export from the A3
638 station sediment trap at 289 m ($98.2 \pm 4.4 \text{ mmol m}^{-2} \text{ y}^{-1}$) falls near annual estimates from deep
639 sediment traps (>2000 m) located in the naturally fertilized area downstream of the Crozet
640 Islands ($37\text{-}60$ and $40\text{-}42 \text{ mmol m}^{-2} \text{ y}^{-1}$, Salter et al., 2012) where fluxes were considered as
641 mainly driven by resting spores of *Eucampia antarctica* var. *antarctica*. ~~The frequent~~
642 ~~occurrence and widespread distribution of diatoms resting spores suggest their pivotal role in~~
643 ~~the efficient transfer of carbon to depth. Although they are 20 frequently observed in blooms~~
644 ~~heavily influenced by the proximity of the coast, large scale advection might explain that their~~
645 ~~impact on carbon export is not restricted to neritic areas.~~ Diatom resting spores are frequently
646 observed in blooms heavily influenced by the proximity of the coast. Major resting spores
647 contribution to carbon fluxes was observed in only one study in the open North Atlantic
648 Ocean (Rynearson et al., 2013), but they are generally absent or very rare in open ocean
649 sediment trap studies (Fischer et al., 2002; Grigorov et al., 2014; Rigual-Hernández et al.,
650 2015). The frequent occurrence and widespread distribution of diatoms resting spores in the
651 neritic or coastal-influenced ocean suggest their pivotal role in the efficient transfer of carbon
652 to depth in these areas.

653 *Chaetoceros* resting spores have been reported to contain up to 10 times more carbon
654 than the vegetative forms (Kuwata et al., 1993) with no vacuole and high contents of lipids
655 and carbohydrates (Doucette and Fryxell, 1983; Kuwata et al., 1993). Moreover, CRS resist
656 grazing and have been found to lower copepods grazing pressure (Kuwata and Tsuda, 2005).
657 We suggest that diatom resting spores gather three essential characteristics for **effective**

658 **intense** POC export to the deep ocean: (1) they efficiently bypass the grazing pressure near the
659 mixed layer due to their morphological characteristics such as very robust frustules (CRS) or
660 numerous spines (TRS) (high export efficiency), (2) they are efficiently transferred to depth
661 due to the thick and dense frustule increasing sinking velocity and (3) their high carbon
662 content is protected from microbial degradation by the thick frustules (these last two points
663 result in a high transfer efficiency). The spatial distribution and formation of resting spores
664 may therefore be an integral ecological component defining the strength and efficiency of the
665 biological pump **in specific regions**. Nutrient depletion has been shown to trigger resting spore
666 formation in *Chaetoceros Hyalochaete* laboratory cultures (Garrison, 1981; Sanders and
667 Cibik, 1985; Kuwata et al., 1993; Oku and Kamatani, 1997) over relatively rapid timescales
668 (6 to 48 h, McQuoid and Hobson, 1996). Although Si(OH)_4 depletion appears to be the most
669 likely biogeochemical trigger at the Kerguelen Plateau (from $24 \mu\text{mol L}^{-1}$ in early spring to 2
670 $\mu\text{mol L}^{-1}$ in summer; (Mosseri et al., 2008; Closset et al., 2014)), other environmental factors
671 (iron or light availability) could influence the resting spore formation. **Notably, dissolved iron**
672 **concentration in the mixed layer rapidly decreases to $0.1\sim 0.2 \text{ nmol L}^{-1}$ after the beginning of**
673 **the spring bloom at A3, however the vertical entrainment is much weaker in summer**
674 **compared to spring (Bowie et al., 2014)**. Further work to establish seasonal dynamics of these
675 factors linked to diatom life cycles and specifically **the formation of resting spore formation**
676 **response** is necessary.

677 **4.2 Contribution of faecal pellets to POC flux**

678 Although diatoms resting spores are the primary vector for POC flux below the mixed
679 layer, faecal pellets were also important and accounted for 34.3 % of annual export. It **could**
680 **be has been** hypothesized that faecal pellets are the dominant flux component in High
681 Biomass, Low Export (HBLE) environments, where biomass is routed to higher trophic levels
682 (Lam and Bishop, 2007; Ebersbach et al., 2011). However, this hypothesis does not appear to

683 be true for the bloom of the central Kerguelen Plateau suggesting that faecal material is
684 efficiently reprocessed in the mixed layer, or that a significant part of the pellet flux is
685 excreted below the trap depth by vertically migrating zooplankton. Small spherical faecal
686 pellets dominated the annual numerical faecal pellet flux (53.8 %, Table 6). The short and
687 intense export of small spherical faecal pellets was concomitant with the first strong POC
688 export in cup #4 (December 2011, Table 6). The significance of small spherical faecal pellets
689 to POC flux is somewhat uncharacteristic in comparison to other sediment trap records in
690 shallow areas of the Southern Ocean (Schnack-Schiel and Isla, 2005). They are possibly
691 produced by small cyclopoid copepods, like *Oithona similis* that are abundant in the POOZ
692 (Fransz and Gonzalez, 1995; Pinkerton et al., 2010). More specifically, *O. similis* represents
693 >50 % of mesozooplankton abundance at A3 in spring (Carlotti et al., 2015) ~~have~~-has been
694 observed at station A3 in summer (Carlotti et al., 2008). *Oithona* species are known to be
695 coprophagous and play an important role in flux reprocessing (Gonzalez and Smetacek,
696 1994), which may partially contribute to the rapid flux attenuation observed by efficiently
697 retaining carbon in the mixed layer. This reprocessing feeding strategy might also explain the
698 low faecal pellet flux we observed (highest value of 21.8×10^3 pellet $\text{m}^{-2} \text{d}^{-1}$), which was two
699 orders of magnitude lower than the $>5 \times 10^5$ pellet $\text{m}^{-2} \text{d}^{-1}$ observed in neritic areas where
700 euphausiids dominate the mesozooplankton community (Bodungen, 1986; von Bodungen et
701 al., 1987; Wefer et al., 1988).

702 There ~~are~~-were notable differences in faecal pellet type over the course of the season.
703 The transition from spherical and ovoid pellets in spring to larger cylindrical and tabular
704 pellets in summer presumably reflects shifts in dominant zooplankton species from small
705 cyclopoid copepods towards larger calanoid copepods, euphausiids and salps (e.g. Wilson et
706 al., 2013). Carlotti et al. (2015) report that mesozooplankton biomass doubled between
707 October and November 2011 and was three-fold higher in January 2005 (Carlotti et al., 2008).

708 In spring, [Carlotti et al. \(2015\)](#) observed that the small size fraction (300 – 500 µm) was
709 numerically dominated by *Oithona similis* (50 % of the total mesozooplankton assemblage),
710 although the larger size fractions dominated the mesozooplankton biomass (dominated by
711 *Clausocalanus citer*, and *Rhicalanus gigas*). This is consistent with the dominance of small
712 spherical faecal pellets and the lower contribution of cylindrical shapes we observed in spring
713 and early summer (cups #1 to #4, [October to December 2011](#), Table 6). In summer (January
714 2005), the mesozooplankton community was more diversified and comprised 21 % of small
715 individuals (*Oithona* sp and *Oncea* sp.), 20 % of medium-sized individuals (*Clausocalanus* sp
716 and *Microcalanus* sp.) and 21 % of large individuals (*Calanus* sp., *Metrida* sp., *Paraeuchaeta*
717 sp., *Pleuromama* sp. and *Rhincalanus* sp.; Carlotti et al., 2008). As the median size of faecal
718 pellets increases, so does their relative contribution to carbon flux (Fig. 5b and 5d, Table 6).
719 Our observation of an increasing contribution of cylindrical faecal pellet shapes in summer
720 (cups #5 to #10, [December 2011 to February 2012](#), Table 6) is consistent with the increasing
721 contribution of large calanoid copepods to the mesozooplankton assemblages. We note that
722 pteropods showed the highest contribution to mesozooplankton assemblages at station A3 in
723 summer (16 % of total abundance, Carlotti et al., 2008). We associate this observation with
724 the large ellipsoid faecal pellet shape that was first observed in the sediment trap in cup #5
725 (end December 2011) and represented the highest contribution to faecal pellet carbon fluxes
726 in cup #9 (January/February 2012, Table 7). Tabular faecal pellets dominated the low POC
727 fluxes observed in the autumn and winter when chlorophyll *a* concentration was reduced to
728 background levels, although this interpretation should be taken with caution since a constant
729 and high carbon content was used for this shape. The increase in organic carbon content and
730 negative correlation between the abundance of cylindrical, ellipsoid and tabular faecal pellets
731 fluxes and the BSi:POC molar ratio suggests that large zooplankton producing these tabular
732 pellets (large copepods, euphausiids and salps) ~~are~~ were not feeding directly on diatoms.

733 During the autumn and winter, microbial components other than diatoms must sustain the
734 production of ~~this~~ these large zooplankton. Direct observation of faecal pellet content is
735 beyond the scope of the present study but would help to elucidate how seasonal trends of
736 zooplankton feeding ecology influence carbon and biomineral export. Moreover, dedicated
737 studies are still needed to document the seasonal dynamic of euphausiids and salps
738 abundances over the Kerguelen Plateau to compare them with our reported faecal pellet
739 fluxes.

740 **4.3 Diatom fluxes**

741 The diatom fluxes (sum of empty and full cells) observed at the central Kerguelen
742 Plateau reached their maximum value of 1.2×10^8 cells $\text{m}^{-2} \text{d}^{-1}$ during the two short export
743 events, which is equivalent to 2.4×10^8 valves $\text{m}^{-2} \text{d}^{-1}$. This latter value falls between the
744 highest values observed in POOZ ($\sim 10^7$ valves $\text{m}^{-2} \text{d}^{-1}$ Abelmann and Gersonde, 1991; Salter
745 et al., 2012; Grigorov et al., 2014) and the SIZ ($>10^9$ valves $\text{m}^{-2} \text{d}^{-1}$, Suzuki et al., 2001;
746 Pilskaln et al., 2004). The ~~values~~ diatom fluxes over the Kerguelen plateau are similar to the
747 $2.5 - 3.5 \times 10^8$ valves $\text{m}^{-2} \text{d}^{-1}$ measured at 200 m depth in a coastal station of the Antarctic
748 Peninsula, where CRS represented ~ 80 % of the phytoplankton assemblage (Leventer, 1991).
749 ~~Although the~~ Previous studies report the presence of a resting spore formation strategy in
750 diatom species as typically associated with neritic areas (Smetacek, 1985; Crosta et al., 1997;
751 Salter et al., 2012). ~~their very high export and transfer efficiency together with advection can~~
752 ~~explain their contribution to deep open ocean fluxes (e.g. Rynearson et al., 2013).~~ During a
753 ~~previous the first multidisciplinary process study of the Kerguelen Plateau~~ the summer
754 KEOPS1 cruise, a shift in plankton community composition was observed at station A3
755 between January and February. The surface community initially dominated by *Chaetoceros*
756 *Hyalochaete* vegetative chains gave way to one dominated by *Eucampia antarctica* var.
757 *antarctica*, concomitant with increasing CRS abundance in the mixed layer (Armand et al.,

758 2008a). The abundance of dead cells (within chains or as empty single cells and half cells) in
759 the surface water column also increased from January to February, suggesting intense
760 heterotrophic activity. Surface sediments at station A3 contain, in decreasing abundance, *F.*
761 *keruelensis*, CRS and *T. nitzschioides* spp. cells (Armand et al., 2008b). These sedimentary
762 distributions are consistent with the dominant species observed in the sediment trap, *F.*
763 *keruelensis* and *T. nitzschioides* spp. being present throughout the year and mostly
764 represented by empty cells whereas CRS are exported during short and intense events.

765 *Eucampia antarctica* var. *antarctica* resting spores dominated the deep (2000 m)
766 sediment trap diatom assemblages in the naturally fertilized area close to the Crozet Islands
767 with fluxes $> 10^7$ cells $m^{-2} d^{-1}$ (Salter et al., 2012). We observed highest *Eucampia antarctica*
768 var. *antarctica* full cells fluxes of $\sim 10^6$ cells $m^{-2} d^{-1}$ in summer, which represents $< 10\%$ of the
769 total cell flux. Both vegetative and resting stages were observed. Our results suggest that
770 *Eucampia antarctica* var. *antarctica* is unlikely to be a major driving vector for carbon fluxes
771 to depth over the central Kerguelen Plateau, in part because the community was not forming
772 massive highly-silicified, fast-sinking resting spores contrary to observations near the Crozet
773 Islands. Moreover their biogeographic abundance distribution from sea floor observations
774 suggests they are not dominant in this region of the plateau (Armand et al., 2008b). The iron-
775 fertilized Crozet bloom is north of the Polar Front and dissolved $Si(OH)_4$ concentrations were
776 depleted to $0.2 \mu mol L^{-1}$ (Salter et al., 2007) compared to $\sim 2 \mu mol L^{-1}$ on the Kerguelen
777 Plateau (Mosseri et al., 2008). It is possible, along with differences in iron dynamics between
778 the two plateaus, that differences in nutrient stoichiometry favour bloom dynamics and resting
779 spore formation of *Chaetoceros Hyalochaete* populations surrounding the Kerguelen Islands.
780 Nevertheless, the increasing full cell flux of *Eucampia antarctica* var. *antarctica* from spring
781 to summer in the sediment trap time series is consistent with the observations of an increasing

782 abundance in the mixed layer at the station A3 in summer (Armand et al., 2008a). ~~and~~
783 ~~therefore the role this species plays as an efficient vector for carbon export.~~

784 Highest *Pseudo-nitzschia* spp. full cell fluxes were observed in summer,
785 concomitantly with the second export ~~peak event~~ (cup #9, ~~end January 2012~~). *Pseudo-*
786 *nitzschia* species are rarely found in deep sediment trap studies and are absent from ~~the~~
787 sediment diatom assemblages, ~~presumably~~ due to their susceptibility to ~~water column~~
788 dissolution (Grigorov et al., 2014; Rigual-Hernández et al., 2015). ~~The species *Pseudo-*~~
789 ~~*nitzschia hemii* has been reported to accumulate in summer in deep chlorophyll maximum in~~
790 ~~the Polar Frontal Zone (Kopczynska et al., 2001). Such deep biomass accumulation is~~
791 ~~hypothesized to benefit from nutrient diffusion through the pycnocline (Parslow et al., 2001).~~
792 ~~These general observations are consistent with the peaks in *Pseudo-nitzschia* spp. fluxes we~~
793 ~~report in summer over the Kerguelen Plateau. The genera have been reported to accumulate in~~
794 ~~summer in deep chlorophyll maximum, benefiting from nutrient diffusion through the~~
795 ~~pycnocline (Parslow et al., 2001) This ecological characteristic, together with the shallow~~
796 ~~sediment trap depth (289 m) may explain our observations of peaks in *Pseudo-nitzschia* spp.~~
797 ~~fluxes during summer.~~

798 Although their fluxes were very low, species of the *Rhizosolenia* and *Proboscia* ~~genus~~
799 ~~genera~~ were mostly exported as empty cells at the end of summer and during autumn (cups #8
800 to #11, ~~end January to May 2012~~), occurring in parallel with the full cell fluxes of the giant
801 diatom *Thalassiothrix antarctica* (Table 4). It has been suggested that these species belong to
802 a group of “deep shade flora” that accumulate at the subsurface chlorophyll maxima in
803 summer with their ~~highly silicified~~, large frustules protecting them from grazing pressure ~~in~~
804 ~~stratified waters~~ (Kemp and Villareal, 2013). Interestingly these species were also found in
805 deep sediment traps located in a ~~non-fertilized~~ HNLC area ~~south of the Crozet Plateau~~ (Salter
806 et al., 2012), as well as in subsurface chlorophyll maximum in HNLC waters of the Southern

807 Ocean (Parslow et al., 2001; Holm-Hansen et al., 2004; Gomi et al., 2010). A subsurface
808 chlorophyll maximum has previously been observed at 120 m on the Kerguelen Plateau (also
809 station A3) during summer (Uitz et al., 2009) and appears to correspond to an accumulation of
810 particles consisting of aggregates of large diatom species (Jouandet et al., 2011). The fact that
811 *Rhizosolenia* spp. and *Proboscia* spp. were observed as empty cells whereas *Thalassiothrix*
812 *antarctica* was mostly represented by full cells suggest species-specific grazing on these
813 communities. There appears to be ecological differentiation within the “deep shade flora” that
814 precludes describing a single effect on export stoichiometry. Moreover, on the Kerguelen
815 Plateau, these species are not exported in “massive” proportions as the fall-dump hypothesis
816 suggests (Kemp et al., 2000). (~~Kemp and Villareal, 2013~~). The physical and biogeochemical
817 factors responsible for their production and export are still to be determined, and should be
818 investigated thoroughly given the potential importance that these species might have for
819 export fluxes on a global scale (Kemp et al., 2000; Richardson et al., 2000; Kemp and
820 Villareal, 2013).

821 **4.4 Preferential carbon and silica sinkers**

822 Unlike most previous sediment trap studies in the Southern Ocean, we used a counting
823 technique that facilitated the identification of carbon and siliceous components of exported
824 material. Although we lost a small degree of taxonomic resolution with this approach (see
825 methods), it allowed us to avoid unnecessary assumptions concerning carbon content of
826 exported diatoms and directly pinpoint constrain the role of different species for carbon and
827 silica export.

828 The annual BSi:POC ratio of the exported material (1.16) is much higher than the
829 usual ratio proposed for marine diatoms of 0.13 (Brzezinski, 1985). Moreover, the BSi:POC
830 ratio of the exported material in spring (2.1 to 3.4, cups #1 to #3, October to mid-December

831 2011) is significantly higher than the BSi:POC ratio of 0.32 ± 0.06 in the mixed layer of the
832 same station during spring (Lasbleiz et al., 2014). Numerous chemical, physical, biological
833 and ecological factors can impact BSi:POC ratios of marine diatoms (e.g. Ragueneau et al.,
834 2006). However, the ten-fold differences in BSi:POC ratios of exported particles between
835 spring and summer is unlikely to result **simply only** from physiological constraints set during
836 diatoms growth (Hutchins and Bruland, 1998; Takeda, 1998). Previous comparisons in natural
837 and artificially iron-fertilized settings have the highlighted importance of diatom community
838 structure for carbon and silica export (Smetacek et al., 2004; Salter et al., 2012; Quéguiner,
839 2013; Assmy et al., 2013). The presence of different diatom species and their characteristic
840 traits (e. g. susceptibility to grazing, apoptosis, viral lysis) are all likely to influence the flux
841 of full and empty cells. Therefore, the net BSi:POC export ratio results from the net effect of
842 species specific Si:C composition (Sackett et al., 2014) and the subsequent species-specific
843 mortality pathway and dissolution. A significant correlation between BSi:POC and empty:full
844 cells ratio (Spearman rank correlation, $n = 12$, $\rho = 0.78$, $p < 0.05$) suggests the latter acts as a
845 first order control on the silicon and organic carbon export stoichiometry. **Differences in**
846 **BSi:POC ratios between the mixed layer suspended particle stock and particles exported out**
847 **the mixed layer may be explained by the dominant sedimentation of empty diatom frustules**
848 **that results from the grazing pressure by the zooplankton community and the intense carbon**
849 **utilization by heterotrophic microbial communities (Christaki et al., 2014).**

850 We classified species that were observed exclusively as empty cells, or sinking with an
851 integrated empty:full ratio >2 , as predominantly silica exporters and these included: *C.*
852 *bulbosum*, *C. pennatum*, *P. truncata*, *R. antennata/styliformis*, *A. hookeri*, *A. hyalinus*, *C.*
853 *decipiens*, *C. inerme*, *D. antarcticus*, *P. alata*, *T. nitzschoides* spp., *T. lentiginosa*, and small
854 centric species ($< 20 \mu\text{m}$). Although *F. kerguelensis*, *T. nitzschoides* spp. and *T. lentiginosa*
855 were present through the entire season, their fluxes were highly correlated with BSi:POC

856 ratios (Fig. 6) identifying these species as significant contributors to silica export. On the
857 contrary resting spores and species that sink with a major contribution of full cells (integrated
858 empty-full ratio <0.5) were identified as belonging to the preferential carbon sinkers: *C.*
859 *Hyalochaete* spp., *E. antarctica* var. *antarctica*, *R. simplex* and *Thalassiothrix antarctica*.
860 Among them, CRS and *E. antarctica* var. *antarctica* were the most negatively correlated to
861 the BSi:POC ratio and were identified as key species for carbon export (Fig. 6). **These**
862 **observations are consistent with a previous study of natural iron fertilization that identified *C.***
863 ***pennatum*, *D. antarcticus* and *F. kerguelensis* as major silica sinkers and CRS and *E.***
864 ***antarctica* var. *antarctica* resting spores as major carbon sinkers downstream Crozet islands**
865 **(Salter et al., 2012). During the EIFEX artificial fertilization experiment *C. Hyalochaete***
866 **vegetative stages were identified as major carbon sinker whereas *F. kerguelensis* was**
867 **considered as strong silica sinker (Assmy et al., 2013). Notably, resting spore formation was**
868 **not observed in the artificial experiment performed in the open ocean remote from coastal**
869 **influence, and carbon export was attributed to mass mortality and aggregation of algal cells**
870 **(Assmy et al., 2013). Nevertheless, a more detailed analysis of species-specific carbon and**
871 **silica content in the exported material is necessary to fully elucidate their respective roles on**
872 **carbon and silica export.**

873 ~~These observations are consistent with previous studies of natural (Salter et al., 2012)~~
874 ~~and artificial (Assmy et al., 2013) iron fertilization that identified *C. pennatum*, *D. antarcticus*~~
875 ~~and *F. kerguelensis* as major silica sinkers and *C. Hyalochaete* vegetative cells, CRS and *E.*~~
876 ~~*antarctica* var. *antarctica* resting spores as major carbon sinkers. Notably, resting spore~~
877 ~~formation was not observed in the artificial experiment and carbon export was attributed to~~
878 ~~mass mortality and aggregation of algal cells (Assmy et al., 2013). Nevertheless, a more~~
879 ~~detailed analysis of species-specific carbon and silica content in the exported material is~~
880 ~~necessary to fully validate their respective role on carbon and silica export.~~

881

882 **4.5 Seasonal succession of ecological flux vectors over the Kerguelen Plateau**

883 Although sediment trap records integrate cumulative processes of production in the mixed
884 layer and **selective** losses during export, they provide a unique insight into the temporal
885 succession of plankton functional types and resultant geochemical properties of exported
886 particles characterizing the biological pump. **The seasonal cycle of ecological vectors and**
887 **associated export stoichiometry is summarized in Figure 7.** The robustness of the relationship
888 between measured and calculated POC fluxes (**Fig. 8b**) suggests that the main ecological flux
889 vectors described from ~~our sediment trap~~ the samples are ~~sufficient to model the seasonal~~
890 ~~evolution~~ **capable of predicting seasonal patterns** of total POC fluxes (~~Fig. 8b~~). At an annual
891 scale the calculated POC fluxes slightly underestimate ~~those measured~~ **the measured fluxes**
892 (93.1 versus 98.2 mmol m⁻²), ~~which~~ **This** might results from the minor contribution of full
893 cells other than the diatoms species considered, ~~in addition to~~ aggregated material, organic
894 matter sorbed to the exterior of empty cells and faecal fluff that was difficult to enumerate. ~~In~~
895 ~~spring, carbon fluxes are low and mainly associated with the empty cells of small diatoms and~~
896 ~~small faecal pellets. In summer carbon fluxes are primarily driven by resting spores, whereas~~
897 ~~the contribution of small faecal pellets is low. In winter, when primary production is~~
898 ~~negligible, large faecal pellets become the major carbon flux vector.~~

899 **A scheme of phytoplankton and zooplankton communities succession in naturally**
900 **fertilized areas of the Southern Ocean was proposed by Quéguiner (2013). Spring**
901 **phytoplankton communities are characterized by small, lightly silicified, fast growing diatoms**
902 **associated with small microphageous copepods. In summer, the phytoplankton community**
903 **progressively switches toward large, highly silicified, slow growing diatoms resistant to the**
904 **grazing by large copepods. In this scheme carbon export occurs mostly in end summer**
905 **through the fall dump.** The species succession directly observed in our sediment trap samples

906 differs somewhat to the conceptual model ~~of ecological succession in naturally iron fertilized~~
907 ~~areas~~ proposed by Quéguiner (2013), although the general patterns are similar. ~~The first~~
908 ~~diatoms exported in spring are indeed small species of *F. kerguelensis*, *T. nitzschioides* spp.,~~
909 ~~and small centric species (<20 µm).~~ The diatom species exported in spring were *F.*
910 *kerguelensis*, *T. nitzschioides* spp., and small centric species (<20 µm), whilst in summer the
911 comparatively very large (>200 µm) species of *Proboscia* sp., *Rhizosolenia* sp. and
912 *Thalassiothrix antarctica* were observed. However we observe that these species constituting
913 the spring fluxes are exported almost exclusively as empty cells. The abundance of small
914 spherical and ovoid faecal pellet suggests an important role of small copepods in the
915 zooplankton (Yoon et al., 2001; Wilson et al., 2013), which was corroborated by the finding
916 of dominant *Oithona similis* abundances in the spring mesozooplankton assemblages at
917 station A3 (Carlotti et al., 2015). Therefore, our data suggests that spring export captured by
918 the sediment trap was the remnants of a diatom community subject to efficient grazing and
919 carbon utilization in, or at the basis of, the mixed layer, resulting in a BSi:POC export ratio >
920 2 (Table 1).

921 The main difference in our observations and the conceptual scheme of Quéguiner,
922 (2013) is the dominance of *Chaetoceros Hyalochaete* resting spores to diatom export
923 assemblages and their contribution to carbon fluxes out of the mixed layer in summer. ~~;~~
924 ~~probably triggered by Si(OH)₄ limitation.~~ Resting spores appear to efficiently bypass the
925 “carbon trap” represented by grazers and might also physically entrain small faecal pellets in
926 their downward flux. In mid-summer, faecal pellet carbon export is dominated by the
927 contribution of cylindrical shapes. This appears to be consistent with an observed shift toward
928 a higher contribution of large copepods and euphausiids to the mesozooplankton community
929 in the mixed layer (Carlotti et al., 2008). However, CRS still dominate the diatom exported
930 assemblage. The corresponding BSi:POC ratio decreases with values between 1 and 2 (Table

931 1). The fact that there are two discrete resting ~~spore sport~~ export events might be explained by
932 a mixing event that injected Si(OH)₄ into the surface allowing the development of a secondary
933 Si(OH)₄ limitation.

934 In the autumn and winter, diatoms fluxes are very low and faecal pellet carbon export
935 is dominated by cylindrical and tabular contributions consistent with a supposed shift to
936 zooplankton communities dominated by large copepods, euphausiids, and salps (Wilson et al.,
937 2013). The low BSi:POC ratios characterizing export at this time suggest that these
938 communities feed primarily suspended particles (in the case of salps) and on micro- and
939 mesozooplankton or small diatoms, although direct measurements of faecal pellet content
940 would be necessary to confirm this.

941 **5 Conclusion**

942 We report the chemical (particulate organic carbon and nitrogen, biogenic silica) and
943 biological (diatom cells and faecal pellets) composition of material exported beneath the
944 winter mixed layer (289 m) in a naturally iron-fertilized area of the Southern Ocean. ~~Despite~~
945 ~~iron-availability~~, Annually integrated organic carbon export ~~from the iron fertilized bloom~~
946 was low (98 mmol m⁻²) although biogenic silicon export was significant (114 mmol m⁻²).
947 *Chaetoceros Hyalochaete* and *Thalassiosira antarctica* resting spores accounted for more
948 than 60 % of the annual POC flux. The high abundance of empty cells and the low
949 contribution of faecal pellets to POC flux (34 %) suggest efficient carbon retention occurs in,
950 or at the base of the mixed layer. We propose that in this HBLE environment, carbon-rich and
951 fast-sinking resting spores bypass the intense grazing pressure otherwise responsible for the
952 rapid attenuation of flux. The seasonal succession of diatom taxa groups was tightly linked to
953 the stoichiometry of the exported material. Several species were identified as primarily “silica
954 sinkers” e.g. *Fragilariopsis kerguelensis* and *Thalassionema nitzschioides* spp. and others as

955 preferential ‘carbon sinkers’ e.g. resting spores of *Chaetoceros Hyalochaete* and
956 *Thalassiosira antarctica*, *Eucampia antarctica* var. *antarctica* and the giant diatom
957 *Thalassiothrix antarctica*. Faecal pellet types described a clear transition from small spherical
958 shapes (small copepods) in spring, larger cylindrical and ellipsoid shapes in summer
959 (euphausiids and large copepods) and large tabular shape (salps) in fall. Their contribution to
960 carbon fluxes increased with the presence of larger shapes.

961 The change in biological productivity and ocean circulation cannot explain the ~80
962 ppmv atmospheric pCO₂ difference between the preindustrial era and the last glacial
963 maximum (Archer et al., 2000; Bopp et al., 2003; Kohfeld et al., 2005; Wolff et al., 2006).
964 Nevertheless, a simple switch in ‘silica sinker’ versus ‘carbon sinker’ relative abundance
965 would have a drastic effect on carbon sequestration in the Southern Ocean and silicic acid
966 availability at lower latitudes (Sarmiento et al., 2004; Boyd, 2013). The results presented here
967 emphasize the compelling need for similar studies in other locations of the global Ocean that
968 will allow identification of key ecological vectors that set the magnitude and the
969 stoichiometry of the biological pump.

970 **Acknowledgements**

971 We thank the Captain Bernard Lassiette and his crew during the KEOPS2 mission on the R/V
972 *Marion Dufresne II*. We thank Karine Leblanc and Marine Lasbleiz **and three anonymous**
973 **reviewers** for their constructive comments, which helped us to improve the manuscript. This
974 work was supported by the French Research program of INSU-CNRS LEFE-CYBER (Les
975 enveloppes fluides et l’environnement – Cycles biogéochimiques, environnement et
976 ressources), the French ANR (Agence Nationale de la Recherche, SIMI-6 program, ANR-10-
977 BLAN-0614), the French CNES (Centre National d’Etudes Spatiales) and the French Polar

978 Institute IPEV (Institut Polaire Paul-Emile Victor). L. Armand's participation in the KEOPS2
979 program was supported by an Australian Antarctic Division grant (#3214).

- 981 Abdi, H., 2010. Partial least squares regression and projection on latent structure regression (PLS
982 Regression). *Wiley Interdiscip. Rev. Comput. Stat.* 2, 97–106. doi:10.1002/wics.51
- 983 Abelman, A., Gersonde, R., 1991. Biosiliceous particle flux in the Southern Ocean. *Mar. Chem.,
984 Biochemistry and circulation of water masses in the Southern Ocean International Symposium*
985 35, 503–536. doi:10.1016/S0304-4203(09)90040-8
- 986 Allen, C.S., Pike, J., Pudsey, C.J., Leventer, A., 2005. Submillennial variations in ocean conditions
987 during deglaciation based on diatom assemblages from the southwest Atlantic.
988 *Paleoceanography* 20, PA2012. doi:10.1029/2004PA001055
- 989 Aminot, A., Kerouel, R., 2007. Dosage automatique des nutriments dans les eaux marines: méthodes
990 en flux continu. Ifremer, Plouzané, France.
- 991 Archer, D., Winguth, A., Lea, D., Mahowald, N., 2000. What caused the glacial/interglacial
992 atmospheric pCO₂ cycles? *Rev. Geophys.* 38, 159–189. doi:10.1029/1999RG000066
- 993 Armand, L.K., Cornet-Barthaux, V., Mosseri, J., Quéguiner, B., 2008a. Late summer diatom biomass
994 and community structure on and around the naturally iron-fertilised Kerguelen Plateau in the
995 Southern Ocean. *Deep Sea Res. Part II Top. Stud. Oceanogr., KEOPS: Kerguelen Ocean and*
996 *Plateau compared Study* 55, 653–676. doi:10.1016/j.dsr2.2007.12.031
- 997 Armand, L.K., Crosta, X., Quéguiner, B., Mosseri, J., Garcia, N., 2008b. Diatoms preserved in surface
998 sediments of the northeastern Kerguelen Plateau. *Deep Sea Res. Part II Top. Stud. Oceanogr.*
999 55, 677–692. doi:10.1016/j.dsr2.2007.12.032
- 1000 Armand, L.K., Crosta, X., Romero, O., Pichon, J.-J., 2005. The biogeography of major diatom taxa in
1001 Southern Ocean sediments: 1. Sea ice related species. *Palaeogeogr. Palaeoclimatol.*
1002 *Palaeoecol.* 223, 93–126. doi:10.1016/j.palaeo.2005.02.015
- 1003 Arrigo, K.R., Worthen, D., Schnell, A., Lizotte, M.P., 1998. Primary production in Southern Ocean
1004 waters. *J. Geophys. Res. Oceans* 103, 15587–15600. doi:10.1029/98JC00930
- 1005 Assmy, P., Smetacek, V., Montresor, M., Klaas, C., Henjes, J., Strass, V.H., Arrieta, J.M., Bathmann,
1006 U., Berg, G.M., Breitbarth, E., Cisewski, B., Friedrichs, L., Fuchs, N., Herndl, G.J., Jansen, S.,
1007 Krägersky, S., Latasa, M., Peeken, I., Röttgers, R., Scharek, R., Schüller, S.E., Steigenberger,
1008 S., Webb, A., Wolf-Gladrow, D., 2013. Thick-shelled, grazer-protected diatoms decouple
1009 ocean carbon and silicon cycles in the iron-limited Antarctic Circumpolar Current. *Proc. Natl.*
1010 *Acad. Sci.* 110, 20633–20638. doi:10.1073/pnas.1309345110
- 1011 Baker, E.T., Milburn, H.B., Tennant, D.A., 1988. Field assessment of sediment trap efficiency under
1012 varying flow conditions. *J. Mar. Res.* 46, 573–592. doi:10.1357/002224088785113522
- 1013 Bao, R., Stigter, H.D., Weering, T.C.E.V., 2000. Diatom fluxes in surface sediments of the Goban
1014 Spur continental margin, NE Atlantic Ocean. *J. Micropalaeontology* 19, 123–131.
1015 doi:10.1144/jm.19.2.123
- 1016 Blain, S., Quéguiner, B., Armand, L., Belviso, S., Bombled, B., Bopp, L., Bowie, A., Brunet, C.,
1017 Brussaard, C., Carlotti, F., Christaki, U., Corbière, A., Durand, I., Ebersbach, F., Fuda, J.-L.,
1018 Garcia, N., Gerringa, L., Griffiths, B., Guigue, C., Guillermin, C., Jacquet, S., Jeandel, C., Laan,
1019 P., Lefèvre, D., Lo Monaco, C., Malits, A., Mosseri, J., Obernosterer, I., Park, Y.-H., Picheral,
1020 M., Pondaven, P., Remenyi, T., Sandroni, V., Sarthou, G., Savoye, N., Scouarnec, L.,
1021 Souhaut, M., Thuiller, D., Timmermans, K., Trull, T., Uitz, J., van Beek, P., Veldhuis, M.,
1022 Vincent, D., Viollier, E., Vong, L., Wagener, T., 2007. Effect of natural iron fertilization on
1023 carbon sequestration in the Southern Ocean. *Nature* 446, 1070–1074.
1024 doi:10.1038/nature05700
- 1025 Blain, S., Renaut, S., Xing, X., Claustre, H., Guinet, C., 2013. Instrumented elephant seals reveal the
1026 seasonality in chlorophyll and light-mixing regime in the iron-fertilized Southern Ocean.
1027 *Geophys. Res. Lett.* 40, 6368–6372. doi:10.1002/2013GL058065
- 1028 Blain, S., Tréguer, P., Belviso, S., Bucciarelli, E., Denis, M., Desabre, S., Fiala, M., Martin Jézéquel,
1029 V., Le Fèvre, J., Mayzaud, P., Marty, J.-C., Razouls, S., 2001. A biogeochemical study of the
1030 island mass effect in the context of the iron hypothesis: Kerguelen Islands, Southern Ocean.
1031 *Deep Sea Res. Part Oceanogr. Res. Pap.* 48, 163–187. doi:10.1016/S0967-0637(00)00047-9

- 1032 Bodungen, B. von, 1986. Phytoplankton growth and krill grazing during spring in the Bransfield
1033 Strait, Antarctica — Implications from sediment trap collections. *Polar Biol.* 6, 153–160.
1034 doi:10.1007/BF00274878
- 1035 Bopp, L., Kohfeld, K.E., Le Quéré, C., Aumont, O., 2003. Dust impact on marine biota and
1036 atmospheric CO₂ during glacial periods. *Paleoceanography* 18, 1046.
1037 doi:10.1029/2002PA000810
- 1038 Bowie, A.R., van der Merwe, P., Quéroúé, F., Trull, T., Fourquez, M., Planchon, F., Sarthou, G.,
1039 Chever, F., Townsend, A.T., Obernosterer, I., Sallée, J.-B., Blain, S., 2014. Iron budgets for
1040 three distinct biogeochemical sites around the Kerguelen archipelago (Southern Ocean) during
1041 the natural fertilisation experiment KEOPS-2. *Biogeosciences Discuss* 11, 17861–17923.
1042 doi:10.5194/bgd-11-17861-2014
- 1043 Boyd, P.W., 2013. Diatom traits regulate Southern Ocean silica leakage. *Proc. Natl. Acad. Sci.* 110,
1044 20358–20359. doi:10.1073/pnas.1320327110
- 1045 Brzezinski, M.A., 1985. The Si:C:N ratio of marine diatoms: interspecific variability and the effect of
1046 some environmental variables. *J. Phycol.* 21, 347–357. doi:10.1111/j.0022-3646.1985.00347.x
- 1047 Brzezinski, M.A., Pride, C.J., Franck, V.M., Sigman, D.M., Sarmiento, J.L., Matsumoto, K., Gruber,
1048 N., Rau, G.H., Coale, K.H., 2002. A switch from Si(OH)₄ to NO₃⁻ depletion in the glacial
1049 Southern Ocean. *Geophys. Res. Lett.* 29. doi:10.1029/2001GL014349
- 1050 Buesseler, K.O., 1998. The decoupling of production and particulate export in the surface ocean. *Glob.*
1051 *Biogeochem. Cycles* 12, 297–310. doi:10.1029/97GB03366
- 1052 Buesseler, K.O., Antia, A.N., Chen, M., Fowler, S.W., Gardner, W.D., Gustafsson, Ö., Harada, K.,
1053 Michaels, A.F., Rutgers v. d. Loeff, M., Sarin, M., Steinberg, D.K., Trull, T., 2007. An
1054 assessment of the use of sediment traps for estimating upper ocean particle fluxes. *J. Mar. Res.*
1055 65, 345–416.
- 1056 Buesseler, K.O., Steinberg, D.K., Michaels, A.F., Johnson, R.J., Andrews, J.E., Valdes, J.R., Price,
1057 J.F., 2000. A comparison of the quantity and composition of material caught in a neutrally
1058 buoyant versus surface-tethered sediment trap. *Deep Sea Res. Part Oceanogr. Res. Pap.* 47,
1059 277–294. doi:10.1016/S0967-0637(99)00056-4
- 1060 Burd, A.B., Jackson, G.A., 2009. Particle Aggregation. *Annu. Rev. Mar. Sci.* 1, 65–90.
1061 doi:10.1146/annurev.marine.010908.163904
- 1062 Carlotti, F., Jouandet, M.-P., Nowaczyk, A., Harmelin-Vivien, M., Lefèvre, D., Guillou, G., Zhu, Y.,
1063 Zhou, M., 2015. Mesozooplankton structure and functioning during the onset of the Kerguelen
1064 phytoplankton bloom during the Keops2 survey. *Biogeosciences Discuss* 12, 2381–2427.
1065 doi:10.5194/bgd-12-2381-2015
- 1066 Carlotti, F., Thibault-Botha, D., Nowaczyk, A., Lefèvre, D., 2008. Zooplankton community structure,
1067 biomass and role in carbon fluxes during the second half of a phytoplankton bloom in the
1068 eastern sector of the Kerguelen Shelf (January–February 2005). *Deep Sea Res. Part II Top.*
1069 *Stud. Oceanogr., KEOPS: Kerguelen Ocean and Plateau compared Study* 55, 720–733.
1070 doi:10.1016/j.dsr2.2007.12.010
- 1071 Cavan, E.L., Le Moigne, F. a. c., Poulton, A.J., Tarling, G.A., Ward, P., Daniels, C.J., Fragoso, G.,
1072 Sanders, R.J., 2015. Zooplankton fecal pellets control the attenuation of particulate organic
1073 carbon flux in the Scotia Sea, Southern Ocean. *Geophys. Res. Lett.* 2014GL062744.
1074 doi:10.1002/2014GL062744
- 1075 Chang, A.S., Bertram, M.A., Ivanochko, T., Calvert, S.E., Dallimore, A., Thomson, R.E., 2013.
1076 Annual record of particle fluxes, geochemistry and diatoms in Effingham Inlet, British
1077 Columbia, Canada, and the impact of the 1999 La Niña event. *Mar. Geol.* 337, 20–34.
1078 doi:10.1016/j.margeo.2013.01.003
- 1079 Christaki, U., Lefèvre, D., Georges, C., Colombet, J., Catala, P., Courties, C., Sime-Ngando, T., Blain,
1080 S., Obernosterer, I., 2014. Microbial food web dynamics during spring phytoplankton blooms
1081 in the naturally iron-fertilized Kerguelen area (Southern Ocean). *Biogeosciences* 11, 6739–
1082 6753. doi:10.5194/bg-11-6739-2014
- 1083 Closset, I., Lasbleiz, M., Leblanc, K., Quéguiner, B., Cavagna, A.-J., Elskens, M., Navez, J., Cardinal,
1084 D., 2014. Seasonal evolution of net and regenerated silica production around a natural Fe-
1085 fertilized area in the Southern Ocean estimated with Si isotopic approaches. *Biogeosciences*
1086 11, 5827–5846. doi:10.5194/bg-11-5827-2014

- 1087 Cornet-Barthaux, V., Armand, L., Quiguier, B., 2007. Biovolume and biomass estimates of key
1088 diatoms in the Southern Ocean. *Aquat. Microb. Ecol.* 48, 295–308. doi:10.3354/ame048295
- 1089 Crawford, R., 1995. The role of sex in the sedimentation of a marine diatom bloom. *Limnol.*
1090 *Oceanogr.* 40, 200–204.
- 1091 Crosta, X., Pichon, J.-J., Labracherie, M., 1997. Distribution of *Chaetoceros* resting spores in modern
1092 peri-Antarctic sediments. *Mar. Micropaleontol.* 29, 283–299. doi:10.1016/S0377-
1093 8398(96)00033-3
- 1094 Davison, P.C., Checkley Jr., D.M., Koslow, J.A., Barlow, J., 2013. Carbon export mediated by
1095 mesopelagic fishes in the northeast Pacific Ocean. *Prog. Oceanogr.* 116, 14–30.
1096 doi:10.1016/j.pocean.2013.05.013
- 1097 DeMaster, D.J., 1981. The supply and accumulation of silica in the marine environment. *Geochim.*
1098 *Cosmochim. Acta* 45, 1715–1732. doi:10.1016/0016-7037(81)90006-5
- 1099 Doucette, G.J., Fryxell, G.A., 1983. *Thalassiosira antarctica*: vegetative and resting stage chemical
1100 composition of an ice-related marine diatom. *Mar. Biol.* 78, 1–6. doi:10.1007/BF00392964
- 1101 Dubischar, C.D., Bathmann, U.V., 2002. The occurrence of faecal material in relation to different
1102 pelagic systems in the Southern Ocean and its importance for vertical flux. *Deep Sea Res. Part*
1103 *II Top. Stud. Oceanogr., The Southern Ocean II: Climatic Changes and the Cycle of Carbon*
1104 49, 3229–3242. doi:10.1016/S0967-0645(02)00080-2
- 1105 Dunbar, R.B., 1984. Sediment trap experiments on the Antarctic continental margin. *Antarct. J. US*
1106 70–71.
- 1107 Dutkiewicz, S., Follows, M.J., Parekh, P., 2005. Interactions of the iron and phosphorus cycles: A
1108 three-dimensional model study. *Glob. Biogeochem. Cycles* 19, GB1021.
1109 doi:10.1029/2004GB002342
- 1110 Ebersbach, F., Assmy, P., Martin, P., Schulz, I., Wolzenburg, S., Nöthig, E.-M., 2014. Particle flux
1111 characterisation and sedimentation patterns of protistan plankton during the iron fertilisation
1112 experiment LOHAFEX in the Southern Ocean. *Deep Sea Res. Part Oceanogr. Res. Pap.* 89,
1113 94–103. doi:10.1016/j.dsr.2014.04.007
- 1114 Ebersbach, F., Trull, T.W., 2008. Sinking particle properties from polyacrylamide gels during the
1115 Kerguelen Ocean and Plateau compared Study (KEOPS): Zooplankton control of carbon
1116 export in an area of persistent natural iron inputs in the Southern Ocean. *Limnol. Oceanogr.*
1117 53, 212–224. doi:10.4319/lo.2008.53.1.0212
- 1118 Ebersbach, F., Trull, T.W., Davies, D.M., Bray, S.G., 2011. Controls on mesopelagic particle fluxes in
1119 the Sub-Antarctic and Polar Frontal Zones in the Southern Ocean south of Australia in
1120 summer—Perspectives from free-drifting sediment traps. *Deep Sea Res. Part II Top. Stud.*
1121 *Oceanogr.* 58, 2260–2276. doi:10.1016/j.dsr2.2011.05.025
- 1122 Fischer, G., Fütterer, D., Gersonde, R., Honjo, S., Ostermann, D., Wefer, G., 1988. Seasonal
1123 variability of particle flux in the Weddell Sea and its relation to ice cover. *Nature* 335, 426–
1124 428. doi:10.1038/335426a0
- 1125 Fischer, G., Gersonde, R., Wefer, G., 2002. Organic carbon, biogenic silica and diatom fluxes in the
1126 marginal winter sea-ice zone and in the Polar Front Region: interannual variations and
1127 differences in composition. *Deep Sea Res. Part II Top. Stud. Oceanogr.* 49, 1721–1745.
1128 doi:10.1016/S0967-0645(02)00009-7
- 1129 Franz, H.G., Gonzalez, S.R., 1995. The production of *Oithona similis* (Copepoda: Cyclopoida) in the
1130 Southern Ocean. *ICES J. Mar. Sci. J. Cons.* 52, 549–555. doi:10.1016/1054-3139(95)80069-7
- 1131 Garrison, D.L., 1981. Monterey Bay Phytoplankton. II. Resting Spore Cycles in Coastal Diatom
1132 Populations. *J. Plankton Res.* 3, 137–156. doi:10.1093/plankt/3.1.137
- 1133 Gersonde, R., Zielinski, U., 2000. The reconstruction of late Quaternary Antarctic sea-ice
1134 distribution—the use of diatoms as a proxy for sea-ice. *Palaeogeogr. Palaeoclimatol.*
1135 *Palaeoecol.* 162, 263–286. doi:10.1016/S0031-0182(00)00131-0
- 1136 Gleiber, M.R., Steinberg, D.K., Ducklow, H.W., 2012. Time series of vertical flux of zooplankton
1137 fecal pellets on the continental shelf of the western Antarctic Peninsula. *Mar. Ecol. Prog. Ser.*
1138 471, 23–36. doi:10.3354/meps10021
- 1139 Gomi, Y., Fukuchi, M., Taniguchi, A., 2010. Diatom assemblages at subsurface chlorophyll maximum
1140 layer in the eastern Indian sector of the Southern Ocean in summer. *J. Plankton Res.* 32, 1039–
1141 1050. doi:10.1093/plankt/fbq031

1142 Gonzalez, H.E., Smetacek, V., 1994. The possible role of the cyclopid copepod *Oithona* in retarding
1143 vertical flux of zooplankton faecal material. *Mar. Ecol.-Prog. Ser.* 113, 233–246.

1144 Grigorov, I., Rigual-Hernandez, A.S., Honjo, S., Kemp, A.E.S., Armand, L.K., 2014a. Settling fluxes
1145 of diatoms to the interior of the Antarctic circumpolar current along 170 °W. *Deep Sea Res.*
1146 *Part Oceanogr. Res. Pap.* 93, 1–13. doi:10.1016/j.dsr.2014.07.008

1147 Grigorov, I., Rigual-Hernandez, A.S., Honjo, S., Kemp, A.E.S., Armand, L.K., 2014b. Settling fluxes
1148 of diatoms to the interior of the Antarctic circumpolar current along 170 °W. *Deep Sea Res.*
1149 *Part Oceanogr. Res. Pap.* 93, 1–13. doi:10.1016/j.dsr.2014.07.008

1150 Grimm, K.A., Lange, C.B., Gill, A.S., 1996. Biological forcing of hemipelagic sedimentary laminae;
1151 evidence from ODP Site 893, Santa Barbara Basin, California. *J. Sediment. Res.* 66, 613–624.
1152 doi:10.1306/D42683C4-2B26-11D7-8648000102C1865D

1153 Hasle, G.R., Syvertsen, E.E., 1997. Chapter 2 - Marine Diatoms, in: Tomas, C.R. (Ed.), *Identifying*
1154 *Marine Phytoplankton*. Academic Press, San Diego, pp. 5–385.

1155 Hillebrand, H., Dürselen, C.-D., Kirschtel, D., Pollinger, U., Zohary, T., 1999. Biovolume
1156 Calculation for Pelagic and Benthic Microalgae. *J. Phycol.* 35, 403–424. doi:10.1046/j.1529-
1157 8817.1999.3520403.x

1158 Holm-Hansen, O., Kahru, M., Hewes, C.D., Kawaguchi, S., Kameda, T., Sushin, V.A., Krasovski, I.,
1159 Priddle, J., Korb, R., Hewitt, R.P., Mitchell, B.G., 2004. Temporal and spatial distribution of
1160 chlorophyll-a in surface waters of the Scotia Sea as determined by both shipboard
1161 measurements and satellite data. *Deep Sea Res. Part II Top. Stud. Oceanogr.* 51, 1323–1331.
1162 doi:10.1016/j.dsr2.2004.06.004

1163 Holzer, M., Primeau, F.W., DeVries, T., Matear, R., 2014. The Southern Ocean silicon trap: Data-
1164 constrained estimates of regenerated silicic acid, trapping efficiencies, and global transport
1165 paths. *J. Geophys. Res. Oceans* 119, 313–331. doi:10.1002/2013JC009356

1166 Howard, A.G., Coxhead, A.J., Potter, I.A., Watt, A.P., 1986. Determination of dissolved aluminium by
1167 the micelle-enhanced fluorescence of its lumogallion complex. *Analyst* 111, 1379–1382.
1168 doi:10.1039/AN9861101379

1169 Hutchins, D.A., Bruland, K.W., 1998. Iron-limited diatom growth and Si:N uptake ratios in a coastal
1170 upwelling regime. *Nature* 393, 561–564. doi:10.1038/31203

1171 Ichinomiya, M., Gomi, Y., Nakamachi, M., Honda, M., Fukuchi, M., Taniguchi, A., 2008. Temporal
1172 variations in the abundance and sinking flux of diatoms under fast ice in summer near Syowa
1173 Station, East Antarctica. *Polar Sci.* 2, 33–40. doi:10.1016/j.polar.2008.01.001

1174 Jackson, G.A., Burd, A.B., 2001. A model for the distribution of particle flux in the mid-water column
1175 controlled by subsurface biotic interactions. *Deep Sea Res. Part II Top. Stud. Oceanogr., The*
1176 *US JGOFS Synthesis and Modeling Project: Phase 1* 49, 193–217. doi:10.1016/S0967-
1177 0645(01)00100-X

1178 Jackson, G.A., Waite, A.M., Boyd, P.W., 2005. Role of algal aggregation in vertical carbon export
1179 during SOIREE and in other low biomass environments. *Geophys. Res. Lett.* 32, L13607.
1180 doi:10.1029/2005GL023180

1181 Jin, X., Gruber, N., Dunne, J.P., Sarmiento, J.L., Armstrong, R.A., 2006. Diagnosing the contribution
1182 of phytoplankton functional groups to the production and export of particulate organic carbon,
1183 CaCO₃, and opal from global nutrient and alkalinity distributions. *Glob. Biogeochem. Cycles*
1184 20, GB2015. doi:10.1029/2005GB002532

1185 Jouandet, M.P., Blain, S., Metzl, N., Brunet, C., Trull, T.W., Obernosterer, I., 2008. A seasonal carbon
1186 budget for a naturally iron-fertilized bloom over the Kerguelen Plateau in the Southern Ocean.
1187 *Deep Sea Res. Part II Top. Stud. Oceanogr., KEOPS: Kerguelen Ocean and Plateau compared*
1188 *Study* 55, 856–867. doi:10.1016/j.dsr2.2007.12.037

1189 Jouandet, M.-P., Jackson, G.A., Carlotti, F., Picheral, M., Stemmann, L., Blain, S., 2014. Rapid
1190 formation of large aggregates during the spring bloom of Kerguelen Island: observations and
1191 model comparisons. *Biogeosciences* 11, 4393–4406. doi:10.5194/bg-11-4393-2014

1192 Jouandet, M.-P., Trull, T.W., Guidi, L., Picheral, M., Ebersbach, F., Stemmann, L., Blain, S., 2011.
1193 Optical imaging of mesopelagic particles indicates deep carbon flux beneath a natural iron-
1194 fertilized bloom in the Southern Ocean. *Limnol. Oceanogr.* 56, 1130–1140.
1195 doi:10.4319/lo.2011.56.3.1130

- 1196 Kato, M., Tanimura, Y., Matsuoka, K., Fukusawa, H., 2003. Planktonic diatoms from sediment traps
1197 in Omura Bay, western Japan with implications for ecological and taphonomic studies of
1198 coastal marine environments. *Quat. Int.* 105, 25–31. doi:10.1016/S1040-6182(02)00147-7
- 1199 Kemp, A.E., Pike, J., Pearce, R.B., Lange, C.B., 2000. The “Fall dump” — a new perspective on the
1200 role of a “shade flora” in the annual cycle of diatom production and export flux. *Deep Sea*
1201 *Res. Part II Top. Stud. Oceanogr.* 47, 2129–2154. doi:10.1016/S0967-0645(00)00019-9
- 1202 Kemp, A.E.S., Villareal, T.A., 2013. High diatom production and export in stratified waters – A
1203 potential negative feedback to global warming. *Prog. Oceanogr.* 119, 4–23.
1204 doi:10.1016/j.pocean.2013.06.004
- 1205 Kohfeld, K.E., Quéré, C.L., Harrison, S.P., Anderson, R.F., 2005. Role of Marine Biology in Glacial-
1206 Interglacial CO₂ Cycles. *Science* 308, 74–78. doi:10.1126/science.1105375
- 1207 Kocczynska, E.E., Dehairs, F., Elskens, M., Wright, S., 2001. Phytoplankton and microzooplankton
1208 variability between the Subtropical and Polar Fronts south of Australia: Thriving under
1209 regenerative and new production in late summer. *J. Geophys. Res. Oceans* 106, 31597–31609.
1210 doi:10.1029/2000JC000278
- 1211 Kuwata, A., Hama, T., Takahashi, M., 1993. Ecophysiological characterization of two life forms,
1212 resting spores and resting cells, of a marine planktonic diatom. *Mar. Ecol. Prog. Ser.* 102,
1213 245–255.
- 1214 Kuwata, A., Tsuda, A., 2005. Selection and viability after ingestion of vegetative cells, resting spores
1215 and resting cells of the marine diatom, *Chaetoceros pseudocurvisetus*, by two copepods. *J.*
1216 *Exp. Mar. Biol. Ecol.* 322, 143–151. doi:10.1016/j.jembe.2005.02.013
- 1217 Lampitt, R.S., Boorman, B., Brown, L., Lucas, M., Salter, I., Sanders, R., Saw, K., Seeyave, S.,
1218 Thomalla, S.J., Turnewitsch, R., 2008. Particle export from the euphotic zone: Estimates using
1219 a novel drifting sediment trap, 234Th and new production. *Deep Sea Res. Part Oceanogr. Res.*
1220 *Pap.* 55, 1484–1502. doi:10.1016/j.dsr.2008.07.002
- 1221 Lampitt, R.S., Noji, T., Bodungen, B. von, 1990. What happens to zooplankton faecal pellets?
1222 Implications for material flux. *Mar. Biol.* 104, 15–23. doi:10.1007/BF01313152
- 1223 Lampitt, R.S., Salter, I., Johns, D., 2009. Radiolaria: Major exporters of organic carbon to the deep
1224 ocean. *Glob. Biogeochem. Cycles* 23, GB1010. doi:10.1029/2008GB003221
- 1225 Lam, P.J., Bishop, J.K.B., 2007. High biomass, low export regimes in the Southern Ocean. *Deep Sea*
1226 *Res. Part II Top. Stud. Oceanogr.* 54, 601–638. doi:10.1016/j.dsr2.2007.01.013
- 1227 Lam, P.J., Doney, S.C., Bishop, J.K.B., 2011. The dynamic ocean biological pump: Insights from a
1228 global compilation of particulate organic carbon, CaCO₃, and opal concentration profiles from
1229 the mesopelagic. *Glob. Biogeochem. Cycles* 25, GB3009. doi:10.1029/2010GB003868
- 1230 Lange, 1997. Sedimentation patterns of diatoms, radiolarians, and silicoflagellates in Santa Barbara
1231 Basin, California. *Calif. Coop. Ocean. Fish. Investig. Rep.* 38, 161–170.
- 1232 Lange, C.B., Weinheimer, A.L., Reid, F.M.H., Thunell, R.C., 1997. Sedimentation patterns of
1233 diatoms, radiolarians, and silicoflagellates in Santa Barbara Basin, California. *Calif. Coop.*
1234 *Ocean. Fish. Investig. Rep.* 38, 161–170.
- 1235 Lasbleiz, M., Leblanc, K., Blain, S., Ras, J., Cornet-Barthaux, V., Hélias Nunige, S., Quéguiner, B.,
1236 2014. Pigments, elemental composition (C, N, P, and Si), and stoichiometry of particulate
1237 matter in the naturally iron fertilized region of Kerguelen in the Southern Ocean.
1238 *Biogeosciences* 11, 5931–5955. doi:10.5194/bg-11-5931-2014
- 1239 Laurenceau, E.C., Trull, T.W., Davies, D.M., Bray, S.G., Doran, J., Planchon, F., Carlotti, F.,
1240 Jouandet, M.-P., Cavagna, A.-J., Waite, A.M., Blain, S., 2014. The relative importance of
1241 phytoplankton aggregates and zooplankton fecal pellets to carbon export: insights from free-
1242 drifting sediment trap deployments in naturally iron-fertilised waters near the Kerguelen
1243 plateau. *Biogeosciences Discuss* 11, 13623–13673. doi:10.5194/bgd-11-13623-2014
- 1244 Legendre, P., Dr, L.F.J.L., 1998. *Numerical Ecology*, Édition : 2. ed. Elsevier Science, Amsterdam ;
1245 New York.
- 1246 Leventer, A., 1991. Sediment trap diatom assemblages from the northern Antarctic Peninsula region.
1247 *Deep Sea Res. Part Oceanogr. Res. Pap.* 38, 1127–1143. doi:10.1016/0198-0149(91)90099-2
- 1248 Leventer, A., Dunbar, R.B., 1987. Diatom flux in McMurdo Sound, Antarctica. *Mar. Micropaleontol.*
1249 12, 49–64. doi:10.1016/0377-8398(87)90013-2

- 1250 Lopes, C., Mix, A.C., Abrantes, F., 2006. Diatoms in northeast Pacific surface sediments as
1251 paleoceanographic proxies. *Mar. Micropaleontol.* 60, 45–65.
1252 doi:10.1016/j.marmicro.2006.02.010
- 1253 Madin, L.P., 1982. Production, composition and sedimentation of salp fecal pellets in oceanic waters.
1254 *Mar. Biol.* 67, 39–45. doi:10.1007/BF00397092
- 1255 Maiti, K., Charette, M.A., Buesseler, K.O., Kahru, M., 2013. An inverse relationship between
1256 production and export efficiency in the Southern Ocean. *Geophys. Res. Lett.* 40, 1557–1561.
1257 doi:10.1002/grl.50219
- 1258 Martin, J.H., Gordon, R.M., Fitzwater, S.E., 1990. Iron in Antarctic waters. *Nature* 345, 156–158.
1259 doi:10.1038/345156a0
- 1260 Matsumoto, K., Sarmiento, J.L., Brzezinski, M.A., 2002. Silicic acid leakage from the Southern
1261 Ocean: A possible explanation for glacial atmospheric pCO₂. *Glob. Biogeochem. Cycles* 16,
1262 5–1. doi:10.1029/2001GB001442
- 1263 McQuoid, M.R., Hobson, L.A., 1996. Diatom Resting Stages. *J. Phycol.* 32, 889–902.
1264 doi:10.1111/j.0022-3646.1996.00889.x
- 1265 Menden-Deuer, S., Lessard, E.J., 2000. Carbon to volume relationships for dinoflagellates, diatoms,
1266 and other protist plankton. *Limnol. Oceanogr.* 45, 569–579. doi:10.4319/lo.2000.45.3.0569
- 1267 Moore, C.M., Mills, M.M., Arrigo, K.R., Berman-Frank, I., Bopp, L., Boyd, P.W., Galbraith, E.D.,
1268 Geider, R.J., Guieu, C., Jaccard, S.L., Jickells, T.D., La Roche, J., Lenton, T.M., Mahowald,
1269 N.M., Marañón, E., Marinov, I., Moore, J.K., Nakatsuka, T., Oschlies, A., Saito, M.A.,
1270 Thingstad, T.F., Tsuda, A., Ulloa, O., 2013. Processes and patterns of oceanic nutrient
1271 limitation. *Nat. Geosci.* 6, 701–710. doi:10.1038/ngeo1765
- 1272 Moore, J.K., Doney, S.C., Glover, D.M., Fung, I.Y., 2001. Iron cycling and nutrient-limitation patterns
1273 in surface waters of the World Ocean. *Deep Sea Res.* 49, 463–507. doi:10.1016/S0967-
1274 0645(01)00109-6
- 1275 Mortlock, R.A., Froelich, P.N., 1989. A simple method for the rapid determination of biogenic opal in
1276 pelagic marine sediments. *Deep Sea Res. Part Oceanogr. Res. Pap.* 36, 1415–1426.
1277 doi:10.1016/0198-0149(89)90092-7
- 1278 Mosseri, J., Quéguiner, B., Armand, L., Cornet-Barthaux, V., 2008. Impact of iron on silicon
1279 utilization by diatoms in the Southern Ocean: A case study of Si/N cycle decoupling in a
1280 naturally iron-enriched area. *Deep Sea Res. Part II Top. Stud. Oceanogr., KEOPS: Kerguelen
1281 Ocean and Plateau compared Study* 55, 801–819. doi:10.1016/j.dsr2.2007.12.003
- 1282 Nelson, D.M., Brzezinski, M.A., Sigmon, D.E., Franck, V.M., 2001. A seasonal progression of Si
1283 limitation in the Pacific sector of the Southern Ocean. *Deep Sea Res. Part II Top. Stud.
1284 Oceanogr.* 48, 3973–3995. doi:10.1016/S0967-0645(01)00076-5
- 1285 Nelson, D.M., Tréguer, P., Brzezinski, M.A., Leynaert, A., Quéguiner, B., 1995. Production and
1286 dissolution of biogenic silica in the ocean: Revised global estimates, comparison with regional
1287 data and relationship to biogenic sedimentation. *Glob. Biogeochem. Cycles* 9, 359–372.
1288 doi:10.1029/95GB01070
- 1289 Obernosterer, I., Christaki, U., Lefèvre, D., Catala, P., Van Wambeke, F., Lebaron, P., 2008. Rapid
1290 bacterial mineralization of organic carbon produced during a phytoplankton bloom induced by
1291 natural iron fertilization in the Southern Ocean. *Deep Sea Res. Part II Top. Stud. Oceanogr.*
1292 55, 777–789. doi:10.1016/j.dsr2.2007.12.005
- 1293 Oku, O., Kamatani, A., 1997. Resting spore formation of the marine planktonic diatom *Chaetoceros*
1294 *anastomosans* induced by high salinity and nitrogen depletion. *Mar. Biol.* 127, 515–520.
1295 doi:10.1007/s002270050040
- 1296 Onodera, J., Watanabe, E., Harada, N., Honda, M.C., 2014. Diatom flux reflects water-mass
1297 conditions on the southern Northwind Abyssal Plain, Arctic Ocean. *Biogeosciences Discuss*
1298 11, 15215–15250. doi:10.5194/bgd-11-15215-2014
- 1299 Park, J., Oh, I.-S., Kim, H.-C., Yoo, S., 2010. Variability of SeaWiFs chlorophyll-a in the southwest
1300 Atlantic sector of the Southern Ocean: Strong topographic effects and weak seasonality. *Deep
1301 Sea Res. Part Oceanogr. Res. Pap.* 57, 604–620. doi:10.1016/j.dsr.2010.01.004
- 1302 Park, Y.-H., Durand, I., Kestenare, E., Rougier, G., Zhou, M., d’Ovidio, F., Cotté, C., Lee, J.-H.,
1303 2014. Polar Front around the Kerguelen Islands: An up-to-date determination and associated

1304 circulation of surface/subsurface waters. *J. Geophys. Res. Oceans* 119, 6575–6592.
1305 doi:10.1002/2014JC010061

1306 Park, Y.-H., Roquet, F., Durand, I., Fuda, J.-L., 2008. Large-scale circulation over and around the
1307 Northern Kerguelen Plateau. *Deep Sea Res. Part II Top. Stud. Oceanogr.* 55, 566–581.
1308 doi:10.1016/j.dsr2.2007.12.030

1309 Parslow, J.S., Boyd, P.W., Rintoul, S.R., Griffiths, F.B., 2001. A persistent subsurface chlorophyll
1310 maximum in the Interpolar Frontal Zone south of Australia: Seasonal progression and
1311 implications for phytoplankton-light-nutrient interactions. *J. Geophys. Res. Oceans* 106,
1312 31543–31557. doi:10.1029/2000JC000322

1313 Pilskaln, C.H., Manganini, S.J., Trull, T.W., Armand, L., Howard, W., Asper, V.L., Massom, R.,
1314 2004. Geochemical particle fluxes in the Southern Indian Ocean seasonal ice zone: Prydz Bay
1315 region, East Antarctica. *Deep Sea Res. Part Oceanogr. Res. Pap.* 51, 307–332.
1316 doi:10.1016/j.dsr.2003.10.010

1317 Pinkerton, M.H., Smith, A.N.H., Raymond, B., Hosie, G.W., Sharp, B., Leathwick, J.R., Bradford-
1318 Grieve, J.M., 2010. Spatial and seasonal distribution of adult *Oithona similis* in the Southern
1319 Ocean: Predictions using boosted regression trees. *Deep Sea Res. Part Oceanogr. Res. Pap.* 57,
1320 469–485. doi:10.1016/j.dsr.2009.12.010

1321 Pollard, R., Lucas, M., Read, J., 2002. Physical controls on biogeochemical zonation in the Southern
1322 Ocean. *Deep Sea Res. Part II Top. Stud. Oceanogr.* 49, 3289–3305. doi:10.1016/S0967-
1323 0645(02)00084-X

1324 Primeau, F.W., Holzer, M., DeVries, T., 2013. Southern Ocean nutrient trapping and the efficiency of
1325 the biological pump. *J. Geophys. Res. Oceans* 118, 2547–2564. doi:10.1002/jgrc.20181

1326 Quéguiner, B., 2013. Iron fertilization and the structure of planktonic communities in high nutrient
1327 regions of the Southern Ocean. *Deep Sea Res. Part II Top. Stud. Oceanogr.* 90, 43–54.
1328 doi:10.1016/j.dsr2.2012.07.024

1329 Ragueneau, O., Savoye, N., Del Amo, Y., Cotten, J., Tardiveau, B., Leynaert, A., 2005. A new method
1330 for the measurement of biogenic silica in suspended matter of coastal waters: using Si:Al
1331 ratios to correct for the mineral interference. *Cont. Shelf Res.* 25, 697–710.
1332 doi:10.1016/j.csr.2004.09.017

1333 Ragueneau, O., Schultes, S., Bidle, K., Claquin, P., Moriceau, B., 2006. Si and C interactions in the
1334 world ocean: Importance of ecological processes and implications for the role of diatoms in
1335 the biological pump. *Glob. Biogeochem. Cycles* 20, GB4S02. doi:10.1029/2006GB002688

1336 Rembauville, M., Salter, I., Leblond, N., Gueneugues, A., Blain, S., 2014. Export fluxes in a naturally
1337 fertilized area of the Southern Ocean, the Kerguelen Plateau: seasonal dynamic reveals long
1338 lags and strong attenuation of particulate organic carbon flux (Part 1). *Biogeosciences Discuss*
1339 11, 17043–17087. doi:10.5194/bgd-11-17043-2014

1340 Richardson, K., Visser, A.W., Pedersen, F.B., 2000. Subsurface phytoplankton blooms fuel pelagic
1341 production in the North Sea. *J. Plankton Res.* 22, 1663–1671. doi:10.1093/plankt/22.9.1663

1342 Rigual-Hernández, A.S., Trull, T.W., Bray, S.G., Closset, I., Armand, L.K., 2015. Seasonal dynamics
1343 in diatom and particulate export fluxes to the deep sea in the Australian sector of the southern
1344 Antarctic Zone. *J. Mar. Syst.* 142, 62–74. doi:10.1016/j.jmarsys.2014.10.002

1345 Romero, O.E., Armand, L., 2010. Marine diatoms as indicators of modern changes in oceanographic
1346 conditions. In: 2nd Edition *The Diatoms: Applications for the Environmental and Earth*
1347 *Sciences*,. Camb. Univ. Press 373–400.

1348 Romero, O.E., Fischer, G., Lange, C.B., Wefer, G., 2000. Siliceous phytoplankton of the western
1349 equatorial Atlantic: sediment traps and surface sediments. *Deep Sea Res. Part II Top. Stud.*
1350 *Oceanogr.* 47, 1939–1959. doi:10.1016/S0967-0645(00)00012-6

1351 Romero, O.E., Lange, C.B., Fisher, G., Treppke, U.F., Wefer, G., 1999. Variability in export
1352 production documented by downward fluxes and species composition of marine planktonic
1353 diatoms: observations from the tropical and equatorial Atlantic., in: *The Use of Proxies in*
1354 *Paleoceanography, Examples from the South Atlantic*. Heidelberg, Berlin, pp. 365–392.

1355 Rynearson, T.A., Richardson, K., Lampitt, R.S., Sieracki, M.E., Poulton, A.J., Lyngsgaard, M.M.,
1356 Perry, M.J., 2013. Major contribution of diatom resting spores to vertical flux in the sub-polar
1357 North Atlantic. *Deep Sea Res. Part Oceanogr. Res. Pap.* 82, 60–71.
1358 doi:10.1016/j.dsr.2013.07.013

1359 Sackett, O., Armand, L., Beardall, J., Hill, R., Doblin, M., Connelly, C., Howes, J., Stuart, B., Ralph,
1360 P., Heraud, P., 2014. Taxon-specific responses of Southern Ocean diatoms to Fe enrichment
1361 revealed by synchrotron radiation FTIR microspectroscopy. *Biogeosciences* 11, 5795–5808.
1362 doi:10.5194/bg-11-5795-2014

1363 Sallée, J.-B., Matear, R.J., Rintoul, S.R., Lenton, A., 2012. Localized subduction of anthropogenic
1364 carbon dioxide in the Southern Hemisphere oceans. *Nat. Geosci.* 5, 579–584.
1365 doi:10.1038/ngeo1523

1366 Salter, I., Kemp, A.E.S., Moore, C.M., Lampitt, R.S., Wolff, G.A., Holtvoeth, J., 2012. Diatom resting
1367 spore ecology drives enhanced carbon export from a naturally iron-fertilized bloom in the
1368 Southern Ocean. *Glob. Biogeochem. Cycles* 26, GB1014. doi:10.1029/2010GB003977

1369 Salter, I., Lampitt, R.S., Sanders, R., Poulton, A., Kemp, A.E.S., Boorman, B., Saw, K., Pearce, R.,
1370 2007. Estimating carbon, silica and diatom export from a naturally fertilised phytoplankton
1371 bloom in the Southern Ocean using PELAGRA: A novel drifting sediment trap. *Deep Sea Res.*
1372 Part II Top. Stud. Oceanogr., The Crozet Natural Iron Bloom and Export Experiment
1373 CROZEX 54, 2233–2259. doi:10.1016/j.dsr2.2007.06.008

1374 Salter, I., Schiebel, R., Ziveri, P., Movellan, A., Lampitt, R., Wolff, G.A., 2014. Carbonate counter pump
1375 stimulated by natural iron fertilization in the Polar Frontal Zone. *Nat. Geosci.* 7, 885–889.
1376 doi:10.1038/ngeo2285

1377 Sancetta, C., 1995. Diatoms in the Gulf of California: Seasonal flux patterns and the sediment record
1378 for the last 15,000 years. *Paleoceanography* 10, 67–84. doi:10.1029/94PA02796

1379 Sanders, J.G., Cibik, S.J., 1985. Reduction of growth rate and resting spore formation in a marine
1380 diatom exposed to low levels of cadmium. *Mar. Environ. Res.* 16, 165–180.
1381 doi:10.1016/0141-1136(85)90136-9

1382 Sarmiento, J.L., Gruber, N., Brzezinski, M.A., Dunne, J.P., 2004. High-latitude controls of
1383 thermocline nutrients and low latitude biological productivity. *Nature* 427, 56–60.
1384 doi:10.1038/nature02127

1385 Schnack-Schiel, S.B., Isla, E., 2005. The role of zooplankton in the pelagic-benthic coupling of the
1386 Southern Ocean. *Sci. Mar.* 39–55.

1387 Smetacek, V., Assmy, P., Henjes, J., 2004. The role of grazing in structuring Southern Ocean pelagic
1388 ecosystems and biogeochemical cycles. *Antarct. Sci.* 16, 541–558.
1389 doi:10.1017/S0954102004002317

1390 Smetacek, V.S., 1985. Role of sinking in diatom life-history cycles: ecological, evolutionary and
1391 geological significance. *Mar. Biol.* 84, 239–251. doi:10.1007/BF00392493

1392 Steinberg, D.K., Goldthwait, S.A., Hansell, D.A., 2002. Zooplankton vertical migration and the active
1393 transport of dissolved organic and inorganic nitrogen in the Sargasso Sea. *Deep Sea Res. Part*
1394 *Oceanogr. Res. Pap.* 49, 1445–1461. doi:10.1016/S0967-0637(02)00037-7

1395 Suzuki, H., Sasaki, H., Fukuchi, M., 2001. Short-term variability in the flux of rapidly sinking
1396 particles in the Antarctic marginal ice zone. *Polar Biol.* 24, 697–705.
1397 doi:10.1007/s003000100271

1398 Suzuki, H., Sasaki, H., Fukuchi, M., 2003. Loss Processes of Sinking Fecal Pellets of Zooplankton in
1399 the Mesopelagic Layers of the Antarctic Marginal Ice Zone. *J. Oceanogr.* 59, 809–818.
1400 doi:10.1023/B:JOCE.0000009572.08048.0d

1401 Takahashi, T., Sweeney, C., Hales, B., Chipman, D., Newberger, T., Goddard, J., Iannuzzi, R.,
1402 Sutherland, S., 2012. The Changing Carbon Cycle in the Southern Ocean. *Oceanography* 25,
1403 26–37. doi:10.5670/oceanog.2012.71

1404 Takeda, S., 1998. Influence of iron availability on nutrient consumption ratio of diatoms in oceanic
1405 waters. *Nature* 393, 774–777. doi:10.1038/31674

1406 Tarling, G.A., Ward, P., Atkinson, A., Collins, M.A., Murphy, E.J., 2012. DISCOVERY 2010: Spatial
1407 and temporal variability in a dynamic polar ecosystem. *Deep Sea Res. Part II Top. Stud.*
1408 *Oceanogr.* 59–60, 1–13. doi:10.1016/j.dsr2.2011.10.001

1409 Taylor, S.R., McClennan, S.M., 1986. The continental crust: Its composition and evolution. *Geol. J.*
1410 21, 85–86. doi:10.1002/gj.3350210116

1411 Thomalla, S.J., Fauchereau, N., Swart, S., Monteiro, P.M.S., 2011. Regional scale characteristics of
1412 the seasonal cycle of chlorophyll in the Southern Ocean. *Biogeosciences* 8, 2849–2866.
1413 doi:10.5194/bg-8-2849-2011

1414 Treppke, U.F., Lange, C.B., Wefer, G., 1996. Vertical fluxes of diatoms and silicoflagellates in the
1415 eastern equatorial Atlantic, and their contribution to the sedimentary record. *Mar.*
1416 *Micropaleontol.* 28, 73–96. doi:10.1016/0377-8398(95)00046-1

1417 Uitz, J., Claustre, H., Griffiths, F.B., Ras, J., Garcia, N., Sandroni, V., 2009. A phytoplankton class-
1418 specific primary production model applied to the Kerguelen Islands region (Southern Ocean).
1419 *Deep Sea Res. Part Oceanogr. Res. Pap.* 56, 541–560. doi:10.1016/j.dsr.2008.11.006

1420 Venables, H., Moore, C.M., 2010. Phytoplankton and light limitation in the Southern Ocean: Learning
1421 from high-nutrient, high-chlorophyll areas. *J. Geophys. Res. Oceans* 115, C02015.
1422 doi:10.1029/2009JC005361

1423 Von Bodungen, B., Fischer, G., Nöthig, E.-M., Wefer, G., 1987. Sedimentation of krill faeces during
1424 spring development of phytoplankton in Bransfield Strait, Antarctica. *Mitt Geol Paläont Inst*
1425 *Univ Hambg. SCOPEUNEP Sonderbd* 62, 243–257.

1426 Weber, T.S., Deutsch, C., 2010. Ocean nutrient ratios governed by plankton biogeography. *Nature*
1427 467, 550–554. doi:10.1038/nature09403

1428 Wefer, G., Fischer, G., 1991. Annual primary production and export flux in the Southern Ocean from
1429 sediment trap data. *Mar. Chem., Biochemistry and circulation of water masses in the Southern*
1430 *Ocean International Symposium* 35, 597–613. doi:10.1016/S0304-4203(09)90045-7

1431 Wefer, G., Fischer, G., Fütterer, D., Gersonde, R., 1988. Seasonal particle flux in the Bransfield
1432 Strait, Antarctica. *Deep Sea Res. Part Oceanogr. Res. Pap.* 35, 891–898. doi:10.1016/0198-
1433 0149(88)90066-0

1434 Wefer, G.G., Fisher, D.K., Fütterer, R., Gersonde, R., Honjo, S., Ostermann, D., 1990. Particle
1435 sedimentation and productivity in Antarctic waters of the Atlantic sector., in: *Geological*
1436 *History of the Polar Oceans: Arctic versus Antarctic.* Kluwer Academic Publishers, The
1437 Netherlands, pp. 363–379.

1438 Westberry, T.K., Behrenfeld, M.J., Milligan, A.J., Doney, S.C., 2013. Retrospective satellite ocean
1439 color analysis of purposeful and natural ocean iron fertilization. *Deep Sea Res. Part Oceanogr.*
1440 *Res. Pap.* 73, 1–16. doi:10.1016/j.dsr.2012.11.010

1441 Wilson, S., E., Ruhl, H.A., Smith Jr, K.L., 2013. Zooplankton fecal pellet flux in the abyssal northeast
1442 Pacific: A 15 year time-series study. *Limnol. Oceanogr.* 58, 881–892.
1443 doi:10.4319/lo.2013.58.3.0881

1444 Wilson, S.E., Steinberg, D.K., Buesseler, K.O., 2008. Changes in fecal pellet characteristics with
1445 depth as indicators of zooplankton repackaging of particles in the mesopelagic zone of the
1446 subtropical and subarctic North Pacific Ocean. *Deep Sea Res. Part II Top. Stud. Oceanogr.* 55,
1447 1636–1647. doi:10.1016/j.dsr2.2008.04.019

1448 Wolff, E.W., Fischer, H., Fundel, F., Ruth, U., Twarloh, B., Littot, G.C., Mulvaney, R., Röthlisberger,
1449 R., de Angelis, M., Boutron, C.F., Hansson, M., Jonsell, U., Hutterli, M.A., Lambert, F.,
1450 Kaufmann, P., Stauffer, B., Stocker, T.F., Steffensen, J.P., Bigler, M., Siggaard-Andersen,
1451 M.L., Udisti, R., Becagli, S., Castellano, E., Severi, M., Wagenbach, D., Barbante, C.,
1452 Gabrielli, P., Gaspari, V., 2006. Southern Ocean sea-ice extent, productivity and iron flux over
1453 the past eight glacial cycles. *Nature* 440, 491–496. doi:10.1038/nature04614

1454 Yoon, W., Kim, S., Han, K., 2001. Morphology and sinking velocities of fecal pellets of copepod,
1455 molluscan, euphausiid, and salp taxa in the northeastern tropical Atlantic. *Mar. Biol.* 139,
1456 923–928. doi:10.1007/s002270100630

1457 Zielinski, U., Gersonde, R., 1997. Diatom distribution in Southern Ocean surface sediments (Atlantic
1458 sector): Implications for paleoenvironmental reconstructions. *Palaeogeogr. Palaeoclimatol.*
1459 *Palaeoecol.* 129, 213–250. doi:10.1016/S0031-0182(96)00130-7

1460

1461 **Table 1.** Sediment trap cup collection dates, seasonal attribution, particulate organic carbon (POC)
 1462 and nitrogen (PON) fluxes, biogenic and lithogenic silicon (BSi and LSi) fluxes and molar ratios. POC
 1463 and PON data from Rembauville et al. (2014). ~~and calculated export fluxes of particulate organic~~
 1464 ~~carbon (POC), particulate organic nitrogen (PON) and biogenic silica (BSi) and molar POC:PON and~~
 1465 ~~BSi:POC.~~

Cup	Cup opening date	Cup closing date	Collection time (days)	Season	Mass flux (mg m ⁻² d ⁻¹)	POC flux (mmol m ⁻² d ⁻¹)	PON flux (mmol m ⁻² d ⁻¹)	BSi Flux (mmol m ⁻² d ⁻¹)	LSi flux (μmol m ⁻² d ⁻¹)	% opal	POC:PON	BSi:POC
1	21/10/2011	04/11/2011	14	Spring	52.2	0.15	0.02	0.51	26.6	65.6	6.80	3.46
2	04/11/2011	18/11/2011	14	Spring	28.1	0.14	0.02	0.30	18.0	70.8	6.09	2.18
3	18/11/2011	02/12/2011	14	Spring	54.1	0.15	0.02	0.51	13.0	63.9	7.33	3.43
4	02/12/2011	12/12/2011	10	Summer	261.3	1.60	0.23	2.60	20.9	66.9	6.95	1.63
5	12/12/2011	22/12/2011	10	Summer	23.1	0.34	0.05	0.21	4.4	62.4	6.87	0.64
6	22/12/2011	01/01/2012	10	Summer	74.8	0.51	0.08	0.37	8.2	32.9	6.70	0.72
7	01/01/2012	11/01/2012	10	Summer	80.5	0.42	0.06	0.55	8.9	46.0	6.73	1.32
8	11/01/2012	25/01/2012	14	Summer	59.8	0.34	0.05	0.50	5.4	56.5	6.94	1.48
9	25/01/2012	08/02/2012	14	Summer	238.7	1.47	0.20	2.19	7.2	61.7	7.38	1.49
10	08/02/2012	22/02/2012	14	Summer	75.8	0.55	0.08	0.72	6.1	64.2	6.97	1.32
11	22/02/2012	31/05/2012	99	Autumn	24.4	0.27	0.03	0.08	1.5	21.5	8.09	0.29
12	31/05/2012	07/09/2012	99	Winter	5.1	0.04	0.01	0.03	2.2	35.0	6.06	0.66
Annual export (mmol m⁻² y⁻¹)						98.2	13.6	114	1.85			

1466

1467

1468

1469 **Table 2.** *Chaetoceros* resting spores (CRS) and *Thalassiosira antarctica* resting spores (TRS)
 1470 measurement and biomass data from station A3 sediment trap covering cups #4 (December
 1471 2011) to #11 (April 2012). For each variable, the range and the mean value (**bold italic**) is
 1472 reported.

Spore type	Number measured	Pervalvar axis (µm)	Apical axis (µm)	Shape *	Cell volume (µm ³)	Volume/Carbon relationship	Cell carbon content (pmolC cell ⁻¹)	Cell carbon content (pgC cell ⁻¹)
CRS	63	3.1 – 8.5	7.2 - 17.4	Cylinder + two cones	116.9 – 1415	0.039 pmolC µm ⁻³ #	5 – 55	55 – 662
		6	12.1		483		19	227
TRS	57	10.2 – 26	25.6 – 35.3	Cylinder + two half sphere	14035 – 48477	C = 10 ^{(0.811 log₁₀(V)) - 0.541} §	56 - 153	672 - 1839
		20.8	32.6		35502		119	1428

1473 * As defined in Hillebrand et al., (1999)

1474 # Data representative of *Chaetoceros pseudocurvisetus* resting spore (Kuwata et al. 1993)

1475 § Equation from Menden-Deuer and Lessard, (2000), where C is the carbon content (pg C)
 1476 and V is the cell volume (µm³)

1477

1478

1479 **Table 3.** Faecal pellet measurement and biomass estimations from Station A3 sediment trap.

1480 For each variable, the range and the mean value (**bold italic**) are reported.

Faecal pellet shape	Number measured	Major axis (µm) (a)	Minor axis (µm) (b)	Volume equation	Volume (µm ³)	Volume/carb on relationship	Faecal pellet carbon content (µmolC pellet ⁻¹)	Faecal pellet carbon content (µgC pellet ⁻¹)
Spherical	4041	11 - 1069		4/3 π (a/2) ³	697 - 6.39 × 10 ⁸		2.09 × 10 ⁻⁶ – 1.91	2.51 × 10 ⁻⁵ - 23
		150			1.77 × 10⁶		5.3 10⁻³	0.06
Ovoid	2047	85 - 1132	10-802	4/3 π (a/2) (b/2) ²	4.45 × 10 ³ - 3.81 × 10 ⁸	0.036 mgC mm ⁻³ *	1.34 × 10 ⁻⁵ – 1.14	1.60 × 10 ⁻⁴ – 13.72
		314	154		3.90 × 10⁶		11.7 × 10⁻³	0.14
Cylindrical	1338	106 - 6152	14-547	π (b/2) ² a	1.63 × 10 ⁴ – 1.45 × 10 ⁹		4.89 × 10 ⁻⁴ – 4.35	5.87 × 10 ⁻⁴ - 52
		981	136		1.43 × 10⁷		0.04	0.51
Ellipsoid	54	301 - 3893	51-1051	4/3 π (a/2) (b/2) ²	4.10 × 10 ⁵ – 2.25 × 10 ⁹		1.2 × 10 ⁻³ – 6.75	0.01 - 81
		1329	413		1.19 × 10 ⁸		0.36	4.28
Tabular	29					Constant, 119 µgC pellet ⁻¹ #	9.92	119

1481 * Gonzalez and Smetacek, (1994)

1482 # Wilson et al. (2013)

1483

Chaetoceros Hyalochaete spp. were only found as resting spores.

Species – taxa group	Cup number												Contribution to annual flux (%)
	1	2	3	4	5	6	7	8	9	10	11	12	
<i>Asteromphalus</i> spp.	0	0.01	0	0.03	0	0	0	0	0.12	0	0	0	0.1
<i>Chaetoceros atlanticus</i> Cleve	0	0	0	0	0	0	0	0	0.07	0	0	0	0.0
<i>Chaetoceros atlanticus</i> f. <i>bulbosus</i> Ehrenberg	0	0	0	0	0	0	0	0	0	0	0	0	0.0
<i>Chaetoceros decipiens</i> Cleve	0	0	0.02	0	0	0	0	0	0.07	0	0	0	0.0
<i>Chaetoceros dictyota</i> Ehrenberg	0	0	0	0.07	0	0	0	0	0.26	0	0	0	0.1
<i>Chaetoceros Hyalochaete</i> spp.	0.70	0	1.95	39.92	7.42	23.04	14.37	15.88	78.29	20.24	0.68	0	80.2
<i>Corethron inerme</i> Karsten	0	0	0	0	0	0	0	0	0.23	0	0	0	0.1
<i>Corethron pennatum</i> Grunow	0	0	0	0	0	0	0	0	0	0	0	0	0.0
<i>Dactylosolen antarcticus</i> Castracane	0	0	0	0.05	0	0	0	0	0.02	0	0	0	0.0
<i>Eucampia antarctica</i> var. <i>antarctica</i> (Castracane) Mangin	0.08	0.03	0.06	0.19	0.08	0.36	0.19	0.65	1.03	0.45	0.08	0.01	1.6
<i>Fragilariopsis kerguelensis</i> (O'Meara) Hustedt	0.88	1.06	0	1.93	0.40	0.13	0.21	0.12	1.40	0	0	0	2.4
<i>Fragilariopsis separanda/rhombica</i> group	0.02	0.16	0	0.68	0.05	0.20	0.13	0.07	1.47	0	0	0	1.1
<i>Guinardia cylindrus</i> (Cleve) Hasle	0	0	0	0	0	0	0	0	0.07	0	0	0	0.0
<i>Leptocylindrus</i> sp.	0	0	0	0.03	0	0	0	0	0	0	0	0	0.0
<i>Membraneis</i> spp.	0.04	0.01	0	0.19	0	0	0.02	0.02	0.02	0	0	0	0.1
<i>Navicula</i> spp.	0	0	0.04	0.64	0	0	0	0.29	0.58	0	0	0	0.6
<i>Odontella weissflogii</i> (Grunow) Grunow	0	0	0	0.08	0	0	0	0	0.05	0	0	0	0.0
<i>Pleurosigma</i> spp.	0.01	0	0	0.22	0.02	0.02	0	0.03	0.96	0.04	0	0	0.5
<i>Proboscia alata</i> (Brightwell) Sundröm	0	0	0	0	0	0	0	0	0.09	0	0	0	0.0
<i>Proboscia inermis</i> (Castracane) Jordan & Ligowski	0	0	0	0.03	0	0	0	0	0.33	0	0	0	0.2
<i>Proboscia truncata</i> (Karsten) Nöthig & Logowski	0	0	0	0	0	0	0	0	0	0	0	0	0.0
<i>Pseudo-nitzschia</i> spp.	0.26	0.02	0.21	1.81	0.08	0.45	1.85	1.56	7.08	0.36	0.02	0	5.6
<i>Rhizosolenia antennata/styliformis</i> group	0	0	0	0	0	0	0	0	0.05	0	0	0	0.0
<i>Rhizosolenia chunii</i> Karsten	0	0	0	0	0.05	0	0	0.03	0.07	0	0	0	0.1
<i>Rhizosolenia crassa</i> Schimper in Karsten	0	0	0	0	0	0	0	0	0	0	0	0	0.0
<i>Rhizosolenia simplex</i> Karsten	0	0	0	0	0	0	0	0	0.07	0	0	0	0.0
<i>Thalassionema nitzschioides</i> spp. Pergallo & Pergallo	1.45	1.48	0.20	4.65	0.28	0.14	0.34	0.72	0.89	0.14	0.05	0.01	4.0
<i>Thalassiosira lentiginosa</i> (Janisch) Fryxell	0.01	0	0	0	0	0	0	0	0	0	0	0	0.0
<i>Thalassiosira</i> spp.	0	0.05	0	0.05	0	0	0	0	0.12	0.05	0	0	0.1
<i>Thalassiosira antarctica</i> resting spore (TRS) Comber	0.04	0	2.19	2.65	0.17	0.14	0.13	0.14	0.12	0	0.01	0	2.1

<i>Thalassiothrix antarctica</i> Schimper ex Karsten	0	0	0	0.02	0.05	0.04	0.34	0.14	0.70	0	0	0	0.5
Small centrics (<20 µm)	0.05	0	0	0.41	0	0	0	0	0.19	0.18	0	0	0.3
Large centrics (>20 µm)	0	0	0.05	0.08	0	0	0	0	0.05	0	0	0	0.1
Total full cells	35.39	28.20	47.18	537.38	85.85	245.20	175.89	196.56	943.88	214.65	8.46	0.22	

1486

1487

<i>Thalassiothrix antarctica</i>	0	0	0	0	0	0.02	0	0	0	0.04	0	0	0.0
Schimper ex Karsten													
Small centrics (<20 µm)	0.48	0.44	2.96	16.87	0.28	0.13	0.17	0.24	0.65	0.20	0.03	0.02	15.7
Large centrics (>20 µm)	0	0.03	0.01	0.20	0	0	0	0	0.16	0.04	0	0	0.3
Total empty cells	8.34	3.28	10.57	61.20	1.12	1.59	3.01	4.43	28.98	5.46	0.59	0.07	

1490

1491

1492 **Table 6.** Total faecal pellet (FP) flux, total faecal pellet carbon flux, median volume and
 1493 carbon flux partitioned among faecal pellets types from station A3 sediment trap.
 1494 Contribution to numerical faecal pellet flux is provided in normal text whereas the
 1495 contribution to faecal pellet carbon flux is reported in **bold italic**.

Cup	Total FP flux (nb m ⁻² d ⁻¹) × 10 ³	Total FP carbon flux (mmol m ⁻² d ⁻¹)	Median volume (10 ⁶ μm ³)	Contribution (%)				
				Spherical	Ovoid	Cylindrical	Ellipsoid	Tabular
1	1.39	0.02	2.07	53.3 36.8	19.7 18.6	27.0 44.6	0.0 0.0	0.0 0.0
2	1.75	0.04	3.55	36.5 22.4	29.7 21.3	33.9 56.3	0.0 0.0	0.0 0.0
3	0.72	<0.01	0.95	62.7 54.5	37.3 45.5	0.0 0.0	0.0 0.0	0.0 0.0
4	21.81	0.48	1.91	76.4 83.1	22.8 15.3	0.8 1.6	0.0 0.0	0.0 0.0
5	5.10	0.12	3.71	26.6 13.8	35.0 18.3	38.3 67.4	0.1 0.5	0.0 0.0
6	2.69	0.15	5.67	28.8 4.6	33.1 10.9	37.9 43.1	0.0 0.0	0.2 41.3
7	2.46	0.12	6.71	15.6 2.5	45.5 16.1	37.1 56.0	1.8 25.3	0.0 0.0
8	2.06	0.20	6.18	37.6 1.9	15.5 2.1	44.2 34.6	2.2 15.8	0.4 45.5
9	1.36	0.09	3.59	40.4 2.8	20.5 4.9	35.4 27.9	3.7 64.4	0.0 0.0
10	1.22	0.03	2.34	56.0 17.7	22.4 9.1	21.3 69.9	0.4 3.3	0.0 0.0
11	0.27	0.13	2.10	38.9 0.4	30.8 0.7	20.3 2.5	5.7 3.9	4.3 92.6
12	0.14	0.06	2.41	18.4 0.4	57.6 2.6	20.3 5.3	0.0 0.0	3.7 91.8
Annually integrated contribution to faecal pellet flux				53.8 17.9	27.3 6.6	17.8 17.3	0.7 7.7	0.4 50.4

1496

1497

1498 **Table 7.** Measured and calculated POC fluxes, and POC flux partitioning among the major
 1499 identified ecological vectors of carbon exported out of the mixed layer at station A3.
 1500 Measured total POC flux from Rembauville et al. (2014). CRS: *Chaetoceros Hyalocahete*
 1501 resting spores, TRS: *Thalassiosira antarctica* resting spore.

Cup	Measured POC flux (mmol m ⁻² d ⁻¹)	Calculated POC flux (mmol m ⁻² d ⁻¹)	Contribution to calculated POC flux (%)								Total faecal pellet
			CRS	TRS	Other diatoms	Spherical faecal pellet	Ovoid faecal pellet	Cylindrical faecal pellet	Ellipsoid faecal pellet	Tabular faecal pellet	
1	0.15	0.05	25.3	8.1	38.6	10.3	5.2	12.5	0.0	0.0	28.0
2	0.14	0.06	0.0	0.0	35.4	14.5	13.7	36.4	0.0	0.0	64.6
3	0.15	0.31	12.1	85.1	1.4	0.8	0.6	0.0	0.0	0.0	1.4
4	1.60	1.62	46.8	19.4	3.9	24.8	4.6	0.5	0.0	0.0	29.8
5	0.34	0.29	48.0	6.9	3.3	5.8	7.7	28.2	0.2	0.0	41.8
6	0.51	0.63	69.7	2.7	3.2	1.1	2.7	10.5	0.0	10.1	24.4
7	0.42	0.43	63.1	3.5	5.8	0.7	4.4	15.4	7.0	0.0	27.5
8	0.34	0.56	54.4	2.9	6.8	0.7	0.8	12.4	5.7	16.3	35.9
9	1.47	1.71	86.8	0.8	7.2	0.1	0.3	1.4	3.3	0.0	5.2
10	0.55	0.44	88.1	0.0	4.3	1.4	0.7	5.4	0.3	0.0	7.7
11	0.27	0.14	9.1	1.2	2.2	0.3	0.6	2.2	3.4	81.0	87.5
12	0.04	0.06	0.0	0.0	0.5	0.4	2.6	5.2	0.0	91.3	99.5
Contribution to annual calculated POC flux (%)			52.1	8.6	5.0	5.1	2.0	5.2	2.2	19.8	34.3

1502

1503 **Figures captions.**

1504 **Figure 1.** a) Time series of the surface chlorophyll *a* concentration averaged in a 100 km
1505 radius around the trap location. **The black line represents the climatology calculated for the**
1506 **period 1997/2013, whilst the green line corresponds to the sediment trap deployment period**
1507 **(2011/2012).** b) POC fluxes (grey bars) and C/N molar ratio (red line) of the exported
1508 material, c) BSi flux (light blue bars) and BSi:POC ratio (blue line). Errorbars are standard
1509 deviation on triplicates.

1510 **Figure 2.** a) Total diatom cells fluxes (bars, left axis) and total empty:full cells ratio (blue
1511 line, right axis). b) to h) Fluxes of diatom cells from selected species identified as major
1512 contributors to diatom fluxes (>1 % of total diatom fluxes). In b), full cells are *Chaetoceros*
1513 *Hyalochaete* resting spores and empty cells are the vegetative stage. Full cell fluxes are
1514 represented by grey bars whereas empty cell fluxes are represented by white bars

1515 **Figure 3.** Factorial map constituted by the first two axes of the correspondence analysis
1516 performed on the full and empty diatom cell fluxes. Red squares are cup projections with cup
1517 numbers specified, blue circles are full cell projections, white circles are empty cell
1518 projections. The size of the markers is proportional to their representation quality in this
1519 factorial map.

1520 **Figure 4.** Annual ratio of empty to full cells for species observed as both forms. The dashed
1521 lines are the 0.5 and 2 ratio values. *Chaetoceros Hyalochaete* spp. full cells were only
1522 observed as resting spores.

1523 **Figure 5.** a) Faecal pellet numerical fluxes partitioned among faecal pellet types, b) boxplot
1524 of faecal pellet volume. On each box, the central mark is the median, the edges of the box are
1525 the first and third quartiles, the whiskers extend to the most extreme data points comprised in
1526 1.5 times the interquartile distance. c) faecal pellet carbon fluxes partitioned between the five

1527 faecal pellet types. The two arrows represent the two strong POC export events (cup #4 and
1528 #9, December 2011 and end January 2012, respectively).

1529 **Figure 6.** Heatmap representation of β correlation coefficients between the biological
1530 variables (empty and full-cell diatom and faecal pellet type fluxes) and the chemical variables
1531 (POC, PON, BSi, POC:PON and BSi:POC) resulting from the partial least square regression.
1532 Blue circles represent full diatom cells, white circles are empty diatom cells. Brown circles
1533 represent the faecal pellet type fluxes. The ~~numbered and~~ alphabetical labels within the
1534 symbols are used to identify the variable projections shown in Fig. 7. CRS: *Chaetoceros*
1535 *Hyalochaete* resting spores, TRS: *Thalassiosira antarctica* resting spores.

1536 **Figure 7.** Projection of the cups (red squares) the biological factors (circles) and the chemical
1537 factors (green diamonds) in the first two latent vectors of the partial least square regression.
1538 Circled ~~numbers labels~~ refers to the full and empty species listed in Fig. 6.

1539 **Figure 8.** a) Grey bars in the background are measured POC fluxes, colored bars in the
1540 foreground are calculated POC fluxes partitioned among the main ecological vectors
1541 identified. b) Regression ($r^2 = 0.72$) between the measured and calculated POC fluxes. The
1542 correlation is highly significant (Spearman rank correlation, $n = 36$, $\rho = 0.84$, $p < 0.001$).
1543 Error bars were generated by increasing/decreasing the carbon/volume conversion factors by
1544 50 %. Black dashed line is the 1:1 relation, red line is the regression line, red dashed lines
1545 denotes the 99 % confidence interval. CRS: *Chaetoceros Hyalochaete* resting spores, TRS:
1546 *Thalassiosira antarctica* resting spores.

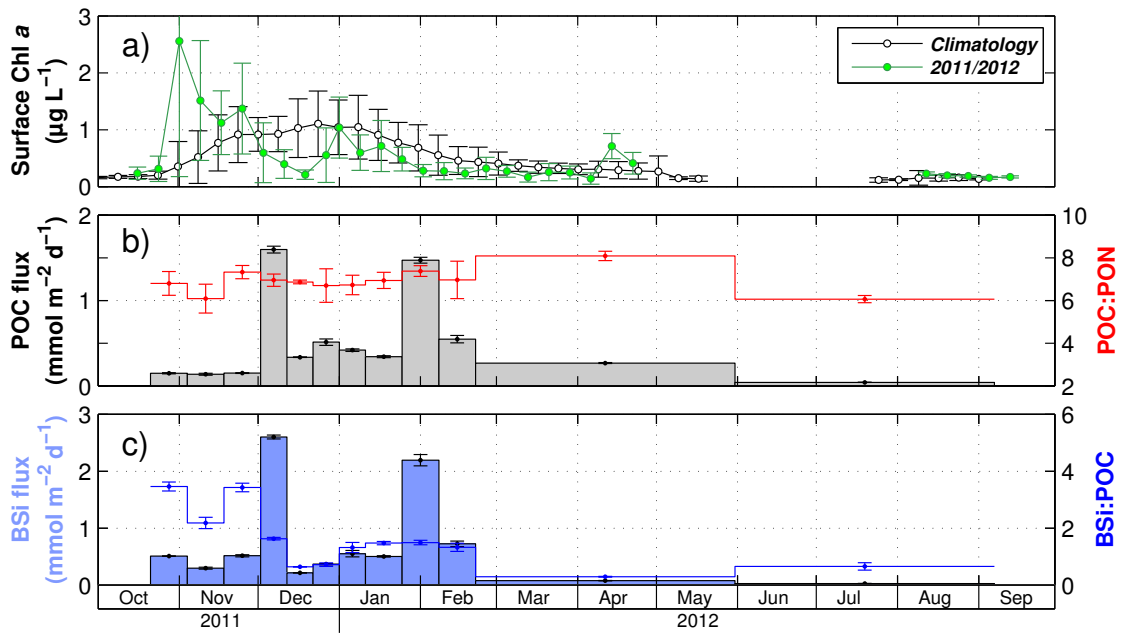


Figure 1.

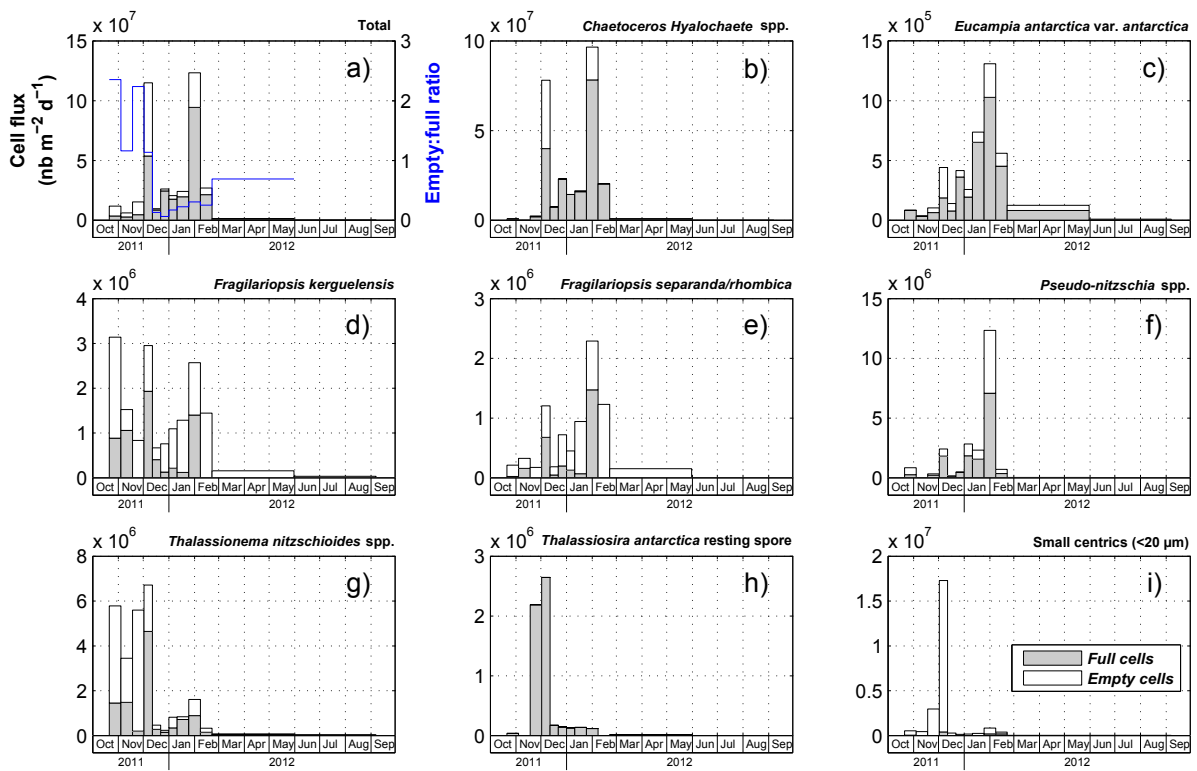


Figure 2.

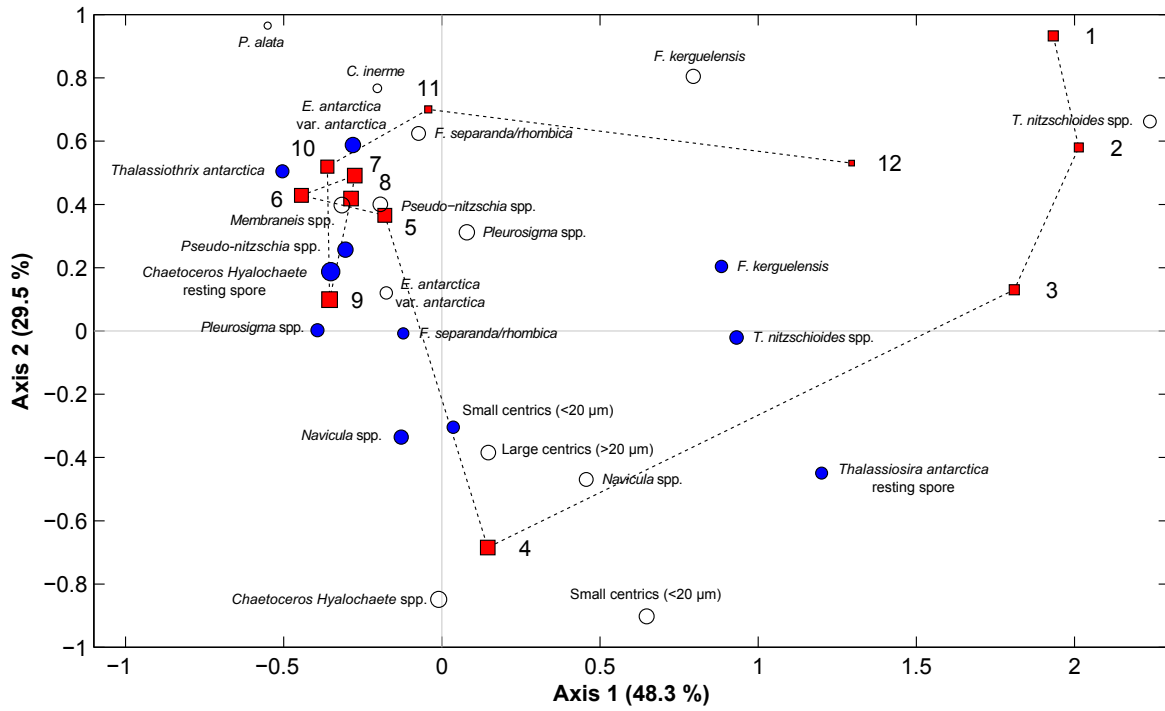


Figure 3.

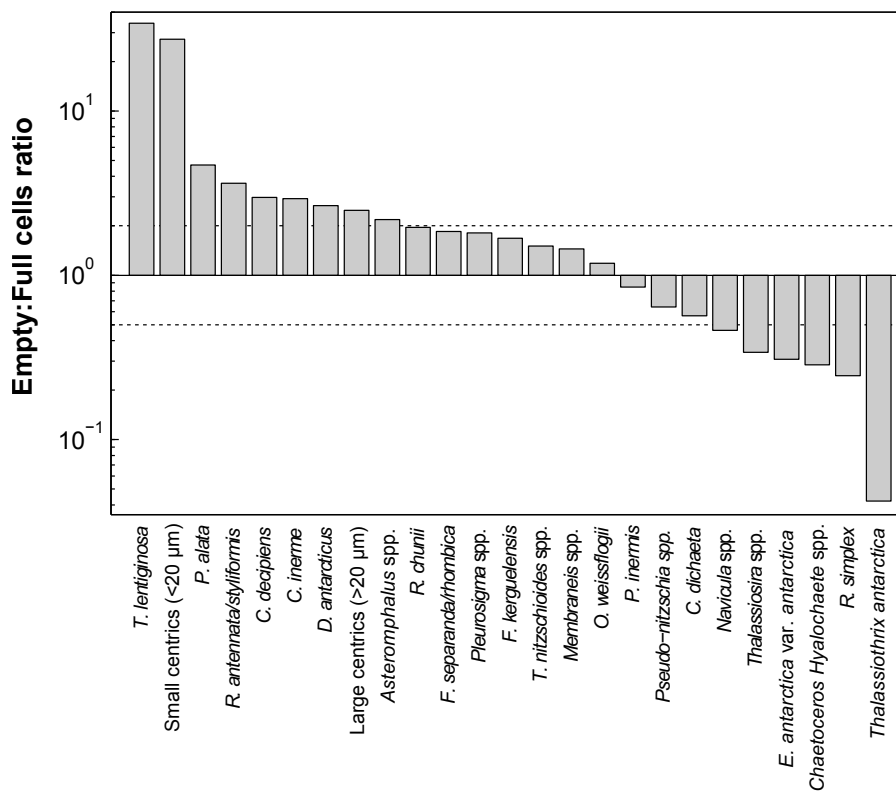


Figure 4.

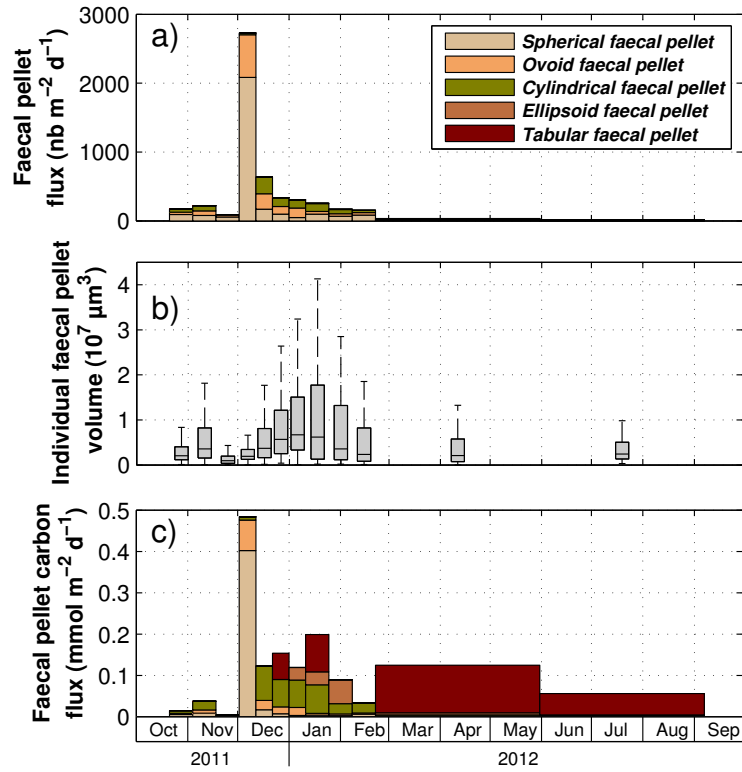


Figure 5.

		POC	PON	BSi	POC:PON	BSi:POC
Ⓐ	CRS	0.07	0.07	0.06	0.02	-0.04
Ⓑ	<i>E. antarctica</i>	0.05	0.05	0.03	0.02	-0.04
Ⓒ	<i>F. kerguelensis</i>	0.05	0.05	0.07	0	0.07
Ⓓ	<i>F. separanda/rhombica</i>	0.06	0.06	0.06	0.02	-0.01
Ⓔ	<i>Navicula</i> spp.	0.07	0.07	0.07	0.02	0
Ⓕ	<i>Pleurosigma</i> spp.	0.06	0.06	0.05	0.02	-0.01
Ⓖ	<i>Pseudo-nitzschia</i> spp.	0.06	0.05	0.05	0.02	-0.01
Ⓗ	<i>T. nitzschioides</i> spp.	0.04	0.04	0.06	0	0.07
Ⓘ	TRS	0.03	0.03	0.05	-0.01	0.1
Ⓚ	<i>Thalassiothrix antarctica</i>	0.04	0.04	0.03	0.01	-0.03
Ⓛ	Small centrics (<20 μm)	0.06	0.06	0.07	0.01	0.01
Ⓜ	<i>Chaetoceros Hyalochaete</i> spp.	0.07	0.07	0.07	0.02	0
Ⓝ	<i>C. inermis</i>	0.03	0.03	0.02	0.01	-0.03
Ⓖ	<i>E. antarctica</i>	0.08	0.07	0.06	0.02	-0.04
Ⓓ	<i>F. kerguelensis</i>	0	0.01	0.05	-0.02	0.17
Ⓔ	<i>F. separanda/rhombica</i>	0.04	0.04	0.03	0.01	-0.03
Ⓕ	<i>Membraneis</i> spp.	0.06	0.06	0.05	0.02	-0.04
Ⓖ	<i>Navicula</i> spp.	0.05	0.05	0.06	0.01	0.05
Ⓗ	<i>Pleurosigma</i> spp.	0.06	0.06	0.06	0.01	0.01
Ⓘ	<i>P. alata</i>	0.01	0.01	0	0.01	-0.03
Ⓚ	<i>Pseudo-nitzschia</i> spp.	0.05	0.05	0.05	0.01	0
Ⓛ	<i>T. nitzschioides</i> spp.	-0.03	-0.02	0.04	-0.04	0.24
Ⓜ	<i>T. lentiginosa</i>	-0.04	-0.04	0.02	-0.04	0.22
Ⓝ	Small centrics (<20 μm)	0.05	0.05	0.06	0.01	0.04
Ⓖ	Large centrics (>20 μm)	0.07	0.07	0.07	0.02	0.01
Ⓓ	Spherical faecal pellet	0.05	0.05	0.05	0.01	0.01
Ⓔ	Ovoid faecal pellet	0.05	0.05	0.04	0.01	-0.02
Ⓕ	Cylindrical faecal pellet	0	0	-0.02	0.01	-0.08
Ⓖ	Ellipsoid faecal pellet	0.03	0.03	0.01	0.01	-0.06
Ⓗ	Tabular faecal pellet	-0.01	-0.01	-0.05	0.02	-0.15

Figure 6.

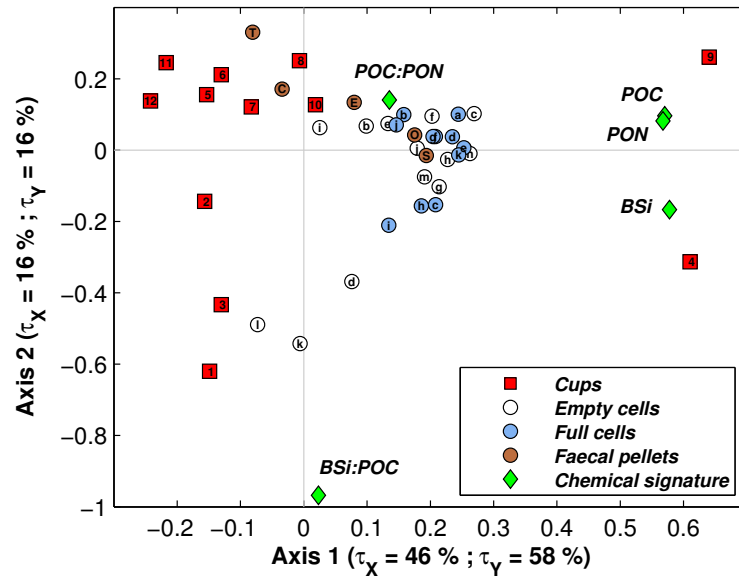


Figure 7.

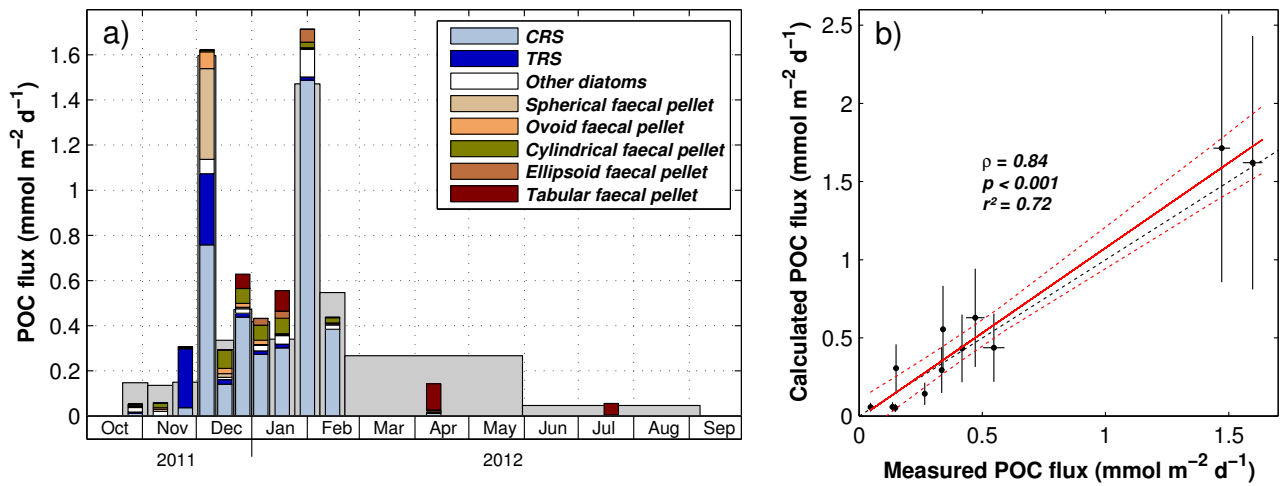


Figure 8.